JACS
JOURNAL OF THE AMERICAN CHEMICAL SOCIETY

ARTICLE

pubs.acs.org/JACS

Self-Repairing Complex Helical Columns Generated via Kinetically Controlled Self-Assembly of Dendronized Perylene Bisimides

Virgil Percec,*[,†] Steven D. Hudson,[⊥] Mihai Peterca,[†,‡] Pawaret Leowanawat,[†] Emad Aqad,[†] Robert Graf,[§] Hans W. Spiess,[§] Xiangbing Zeng,[||] Goran Ungar,[||,#] and Paul A. Heiney[‡]

[†]Roy & Diana Vagelos Laboratories, Department of Chemistry, University of Pennsylvania, Philadelphia, Pennsylvania 19104-6323, United States

[‡]Department of Physics and Astronomy, University of Pennsylvania, Philadelphia, Pennsylvania 19104-6396, United States

[§]Max-Planck Institute for Polymer Research, 55128 Mainz, Germany

[||]Department of Materials Engineering and Science, University of Sheffield, Sheffield S1 3JD, United Kingdom

[⊥]National Institute of Standards and Technology, Gaithersburg, Maryland 20899-8544, United States

[#]WCU C2E2, School of Chemical and Biological Engineering, Seoul National University, Seoul 151-744, Korea

Supporting Information

ABSTRACT: The dendronized perylene 3,4:9,10-tetracarboxylic acid bisimide (PBI), (3,4,5)12G1-3-PBI, was recently reported to self-assemble in complex helical columns containing tetramers of PBI as basic repeat unit. These tetramers contain a pair of two molecules arranged side-by-side and another pair in the next stratum of the column turned upside-down and rotated around the column axis. Intra- and intertetramer rotation angles and stacking distances are different. At high temperature, (3,4,5)12G1-3-PBI self-assembles via a thermodynamically controlled process in a 2D hexagonal columnar phase while at low temperature in a 3D orthorhombic columnar array via a kinetically controlled process. Here, we report the synthesis and structural analysis, by a combination of differential scanning calorimetry, X-ray and electron diffraction, and solid-state NMR performed at different temperatures, on the supramolecular structures generated by a library of (3,4,5)*n*G1-3-PBI with $n = 14-4$. For $n = 11-8$, the kinetically controlled self-assembly from low temperature changes in a thermodynamically controlled process, while the orthorhombic columnar array for $n = 9$ and 8 transforms from the thermodynamic product into the kinetic product. The new thermodynamic product at low temperature for $n = 9, 8$ is a self-repaired helical column with an intra- and intertetramer distance of 3.5 Å forming a 3D monoclinic periodic array via a kinetically controlled self-assembly process. The complex dynamic process leading to this reorganization was elucidated by solid-state NMR and X-ray diffraction. This discovery is important for the field of self-assembly and for the molecular design of supramolecular electronics and solar cell.

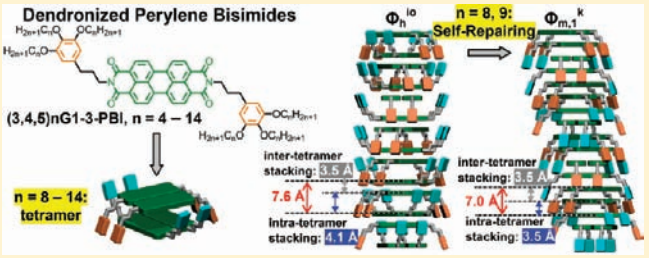

INTRODUCTION

Self-assembling building blocks constructed from perylene 3,4:9,10-tetracarboxylic acid bisimides (PBIs) have emerged in a diversity of supramolecular,[1] macromolecular,[2] and other complex systems[3] that have impacted numerous fields such as industrial dyes and pigments,[4] xerographic receptors,[5] organic semiconductors, transistors, light emitting diodes and solar cells,[1,2] artificial photosynthesis,[3a−c] life science, and biology.[6] PBIs dendronized at the bay[7] and respectively at the imide[8] groups, or at both, provide self-assembling building blocks that are of interest for all of these areas. The functions[9] of all of these molecular and supramolecular assemblies are determined by their two- and three-dimensional (2D and 3D) architectures. Therefore, elucidating the 2D and 3D structure of these functional assemblies and their mechanism[7,8] of formation is crucial for progress in this field.

A previous publication from our laboratory[10] reported the discovery of two novel classes of complex helical columns assembled from PBIs dendronized with first generation self-assembling dendrons containing 0−4 methylenic units (m) between the imide group of the dendron, and 12 methylenic units in their alkyl groups, $n = 12$, (3,4,5)*n*G1-*m*-PBI. The first example of complex helical column is assembled from tetramers containing a pair of two dendronized PBIs arranged side-by-side and another pair in the next stratum of the column, turned upside-down and rotated around the column axis at different angles for different m. This angle is different from the angle between the two pairs forming the tetramer. In this column, the distance between the pairs within a tetramer is different from the distance between tetramers. The second example of complex

Received: September 8, 2011
Published: October 03, 2011

helical column is assembled from dimers consisting of pairs of dendronized PBI arranged on top of each other at a certain angle. The dimers rotate between themselves with a different angle than the angle between the molecules forming the dimer. In this column, the distance between the pair forming the dimer and between the dimers forming the column is equal. Both the complex helical columns assembled from dimers and from tetramers self-organized into 2D-hexagonal columnar phases with intracolumnar order (Φ_h^{io}) at high temperature. At low temperature, the columns generated from tetramers self-organize into a 3D simple orthorhombic lattice (m = 0, 2, 3, 4) ($\Phi_{s\text{-}o}^{k}$), while those from dimers organize into a 3D monoclinic (m = 1) (Φ_m^{k}) periodic array. During the self-assembly in bulk, at high temperature the Φ_h^{io} represents the thermodynamic product. At low temperature, the $\Phi_{s\text{-}o}^{k}$ and Φ_m^{k} are the thermodynamic products. However, the formation of the $\Phi_{s\text{-}o}^{k}$ and Φ_m^{k} phases is so slow that even with rates of cooling of 1 °C/min, sometimes only the Φ_h^{io} phase, which is the kinetic product at low temperature, can be detected. As a consequence, most of the time these 3D complex helical columnar structures could not be detected by a combination of differential scanning calorimetry (DSC) and X-ray diffraction experiments (XRD).[8f,9c,10] Therefore, dendronized PBIs provide extremely interesting examples to investigate the kinetically and thermodynamically controlled self-assembly processes,[11] which, upon elucidation, may have immediate applications in the design of supramolecular electronics and solar cells. For example, an unknown structure obtained by the self-assembly of (3,4,5)12G1-1-PBI displays higher charge carrier mobility than amorphous silicon.[9c] This mobility could have immediate technological applications.

Our laboratory is involved in the investigation of libraries of self-assembling dendrons and dendrimers to discover new supramolecular architectures[12a−l,13] and, subsequently, to predict[12m−o] the primary structure that will generate a particular 3D architecture.

The goal of this Article is to apply for the first time the library approach elaborated previously[12] to self-assembling dendronized PBIs. The first question to address is the following. Is any simple chemical manipulation of the primary structure of a dendronized PBI able to transform the extremely slow rate of assembly of a 3D complex helical column into a fast rate? Or, in other words, is it possible to transform the kinetically controlled self-assembly of the 3D structure from low temperature into a thermodynamically controlled or at least into something close to thermodynamically controlled self-assembly? For the purpose of these experiments, we have selected (3,4,5)12G1-3-PBI as the standard dendronized PBI. The reason for this selection is that the dendronized PBI with n = 12 and m = 3 already displays a sufficiently high rate of formation of its 3D $\Phi_{s\text{-}o}^{k}$ phase.[10] For example, while with heating and cooling rates of 20 and 10 °C/min the $\Phi_{s\text{-}o}^{k}$ phase does not form, this structure starts to become detectable by a combination of DSC and XRD experiments performed with 5 °C/min. This first library approach to dendronized PBIs consists of the synthesis and structural analysis of 11 dendronized PBI with m = 3 and n varying from 14 to 4. The results of this investigation were rewarding. The dendronized PBIs with n = 11, 10, 9, and 8 start to transform the kinetically controlled self-assembly of the $\Phi_{s\text{-}o}^{k}$ phase from low temperature into a thermodynamically controlled process. For these dendronized PBIs, the assembly of their complex helical columns generated from tetramers is almost as fast in the Φ_h^{io} phase as in the $\Phi_{s\text{-}o}^{k}$ phase. However, the central result of these investigations was the most important generated by the structural analysis of this library

Scheme 1. Structure and Schematic of the Self-Assembly Process of Dendronized PBI (3,4,5)*n*G1-*m*-PBI

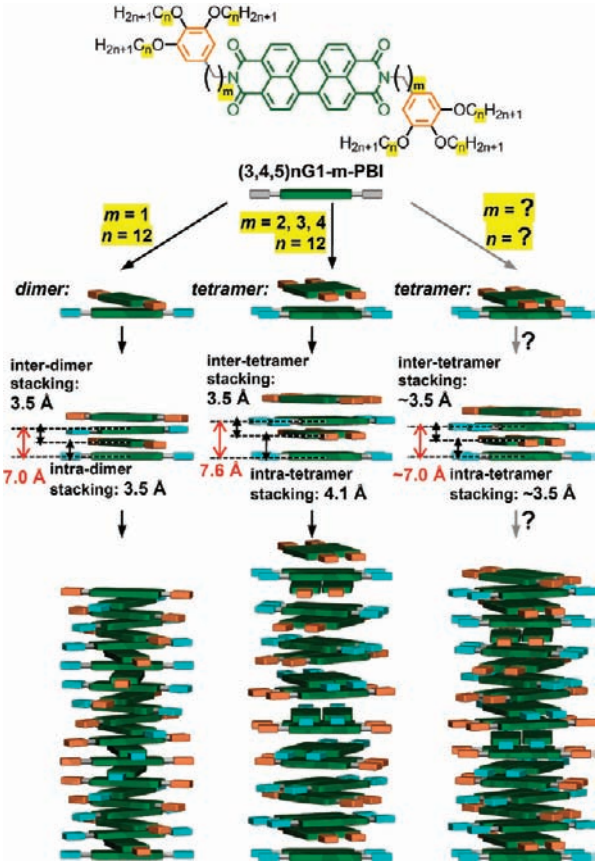

of dendronized PBIs: while annealing in the Φ_h^{io} phase of (3,4,5)9G1-3-PBI, its helical column generated from tetramers of dendronized PBI arranged at an intratetramer distance of 4.1 Å and an intertetramer distance of 3.5 Å[10] self-repairs by a complex dynamic process, elucidated by a combination of XRD and solid-state NMR, and generates a helical column with the intra- and intertetramer stacking of 3.5 Å. This new complex helical column discovered here self-organizes into a new 3D monoclinic ($\Phi_{m,1}^{k}$) periodic array that differs from that reported previously for helical columns assembled from dimers of dendronized PBI.[10] This self-repaired helical column also form in the case of (3,4,5)8G1-3-PBI. The self-repaired column and its corresponding $\Phi_{m,1}^{k}$ phase form only upon annealing in the Φ_h^{io} phase and subsequent cooling from the same phase. The other dendronized PBI with m = 3 and n = 7, 6, 5, and 4 also self-organize into 3D monoclinic ($\Phi_{m,2}^{k}$) phases. However, the structural analysis by XRD suggests that the $\Phi_{m,2}^{k}$ phases are generated by columns containing tilted dendronized PBIs that are not yet elucidated.

RESULTS AND DISCUSSION

Complex Helical Columns Self-Assembled from Dendronized PBI. Scheme 1 describes in a simplified way the structure of the complex helical columns assembled from dimers of dendronized PBI (m = 1; n = 12) (left side) and from tetramers (m = 2, 3, 4; n = 12) (middle).[10] In the case of the helical column generated from dimers, the interdimer and intradimer stacking distances are

Scheme 2. Synthesis of Dendronized PBIs (3,4,5)*n*G1-*m*-PBI with *m* = 3 and *n* = 4−14

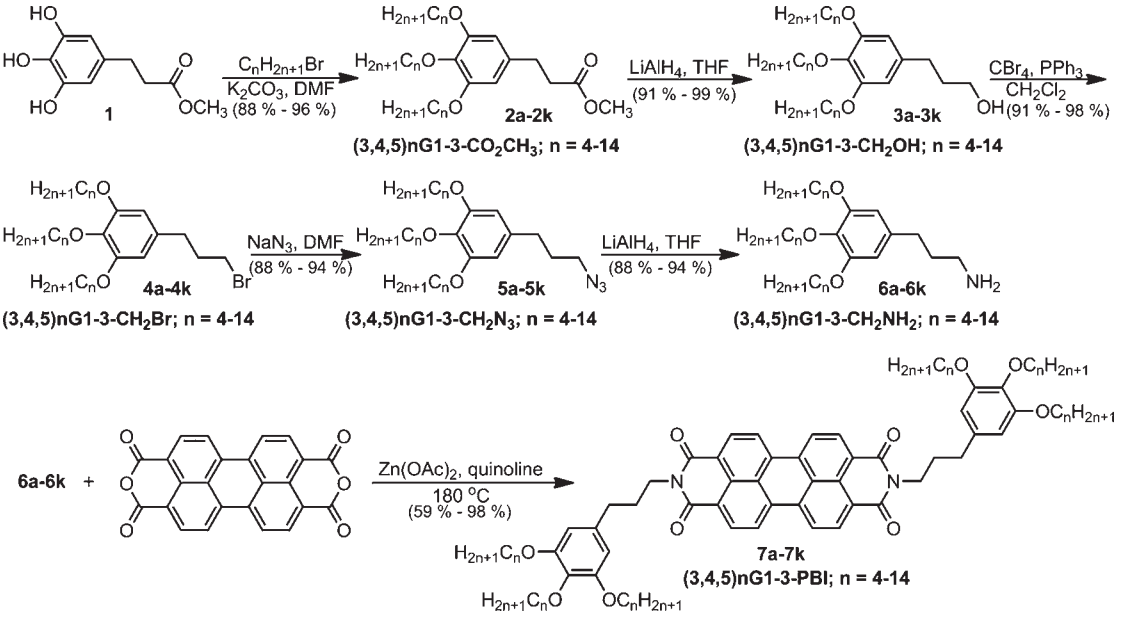

identical and equal to 3.5 Å. In the columns generated from tetramers, the intertetramer stacking is 3.5 Å, while the intratetramer stacking is 4.1 Å. Both the left side and the middle column from Scheme 1 self-organize into 2D Φ_h^{io} phases and into 3D Φ_m^k and $\Phi_{s\text{-}o}^k$ phases. In bulk state, regardless of the heating and cooling rate, at high temperature the Φ_h^{io} phase is the thermodynamic product. At low temperature, the 3D Φ_m^k and $\Phi_{s\text{-}o}^k$ are the thermodynamic products. However, these 3D structures form with very slow rate, usually 1 °C/min, and, therefore, most of the time only the kinetic product, Φ_h^{io}, is observed.[10] The first goal of this research was to search via libraries of dendronized PBIs if the thermodynamically stable structure from low temperature can be generated with high rates of heating and cooling. Ultimately, it will be demonstrated that this is indeed possible. In addition, the same experiments will demonstrate that a self-repairing of the helical column generated from tetramers is also accessible. The self-repaired column will have identical intertetramer and intratetramer stacking distances of 3.5 Å. This is illustrated on the right side column of Scheme 1.

Synthesis of Dendronized PBI. Scheme 2 outlines the synthesis of 11 twin-dendronized[14] PBIs with identical dendrons that differ in the number of methylenic units from the alkyl groups on their periphery from 14 to 4 (n = 14−4). All dendrons are attached to the imide groups of the PBI via three methylenic units (m = 3). Therefore, the short name for this library is (3,4,5)*n*G1-3-PBI. 3-(3,4,5-Trihydroxyphenyl) propionic acid methyl ester, **1**, was synthesized as reported previously[12c] and was alkylated with *n*-alkyl bromides in DMF at 95 °C in the presence of K_2CO_3 to produce **2a**−**2k**, (3,4,5)*n*G1-3-CO_2CH_3 with n = 4−14 in 88−99% yield. Esters **2a**−**2k** were reduced with $LiAlH_4$ in THF at 0 °C for 30 min to produce the dendritic alcohols **3a**−**3k** in 91−95% yield. Bromination of the alcohols **3a**−**3k** with CBr_4/PPh_3[12c] in CH_2Cl_2 at 0 °C for 2 h led to the corresponding bromides **4a**−**4k** (in 91−98% yield), which upon nucleophilic displacement with NaN_3 in DMF at 25 °C for 18 h produced the corresponding azides **5a**−**5k** in 88−94% yield. Reduction of the azides **5a**−**5k** with $LiAlH_4$ in THF at 25 °C for 3 h generated the amines **6a**−**6k** in 88−94% yield. The dendonized PBIs were synthesized in 59−98% yield by a $Zn(OAc)_2$-mediated imidization of perylene 3,4:9,10-tetracarboxylic acid dianhydride in quinoline at 180 °C with 2 equiv of the dendritic amines **6a**−**6k**. The dendronized PBIs **7a**−**7k** were isolated as detailed in the Supporting Information and were purified by column chromatography (silica gel) using CH_2Cl_2/MeOH (100/1) as element followed by precipitation into methanol from CH_2Cl_2 solution. This sequence was repeated until a combination of ^{1}H NMR, ^{13}C NMR, TLC, HPLC, and MALDI-TOF analysis demonstrated >99% purity.

Analysis of Complex Helical Columns and of Their Periodic Arrays via a Combination of DSC and XRD with Different Heating and Cooling Rates. This discussion requires a comparative investigation of Figures 1 and 2. Figure 1 shows first heating DSC scans (left), first cooling scans (middle), and second heating scans (right) recorded with 10 °C/min for all dendronized PBIs synthesized as shown in Scheme 2. Figure 2 illustrates the same DSC traces recorded with 1 °C/min. The identification of all phases was performed by XRD experiments to be discussed in the following sections.

To set the stage for this discussion, we will first recapitulate the phase analysis of (3,4,5)12G1-3-PBI that was reported previously from several laboratories and was analyzed quantitatively for the first time in a recent publication.[10] Let us discuss first the analysis with 10 °C/min (Figure 1). During the first heating scan, the self-organization of this dendronized PBI displays an unknown columnar crystal phase, Φ_x^k, followed by a 2D Φ_h^{io} liquid crystal phase generated from helical columns assembled from tetramers (Scheme 1, middle column). On cooling from the isotropic melt, (i) the Φ_h^{io} phase is observed up to −23 °C when the 2D Φ_h^{io} phase transforms into a 3D columnar hexagonal crystal (Φ_h^k). On second heating scan, the Φ_h^k melts back into the 2D Φ_h^{io} phase, which on further heating transforms into a 3D $\Phi_{s\text{-}o}^k$ phase near an almost undetectable (by DSC) transition to the same

dx.doi.org/10.1021/ja208501d |J. Am. Chem. Soc. 2011, 133, 18479–18494

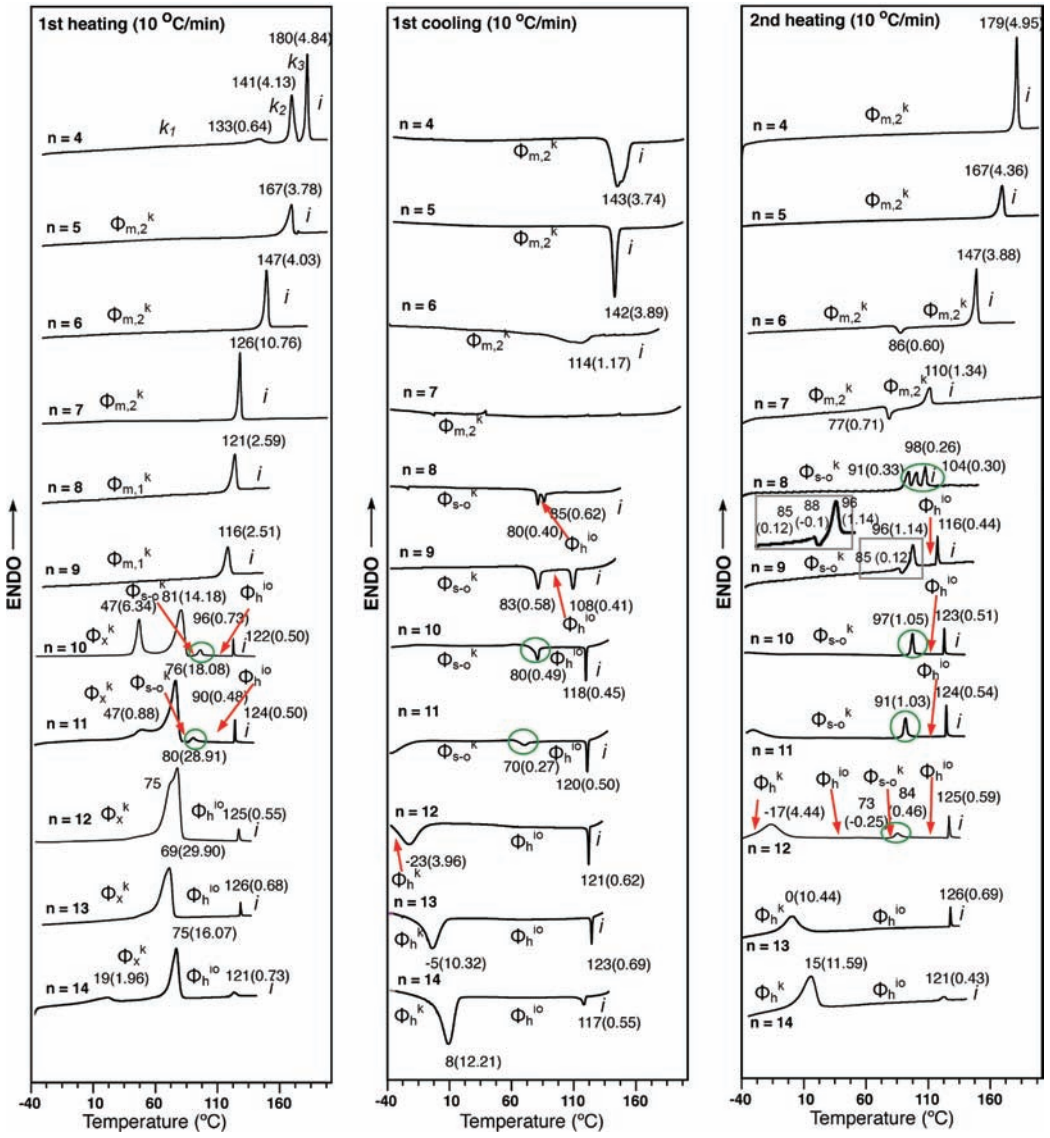

Figure 1. DSC traces of (3,4,5)*n*G1-3-PBI with $n = 14-4$ recorded with heating and cooling rates of 10 °C/min. Phases, transition temperatures, and associated enthalpy changes (in brackets in kcal/mol) are indicated. The green circles mark the transitions dependent on rate.

Φ_h^{io} phase at 84 °C (Figure 1). The 3D $\Phi_{s\text{-}o}^{k}$ phase can be detected only by XRD experiments.

The analysis by DSC recorded with 1 °C/min clarifies the behavior of (3,4,5)12G1-3-PBI (Figure 2). The first heating scan with 1 °C/min (Figure 2) is almost identical to the first heating scan with 10 °C/min (Figure 1). However, the first cooling scan with 1 °C/min differs from the same scan recorded with 10 °C/min. On cooling from the isotropic melt, the Φ_h^{io} phase forms both with 1 °C/min and with 10 °C/min. However, with 1 °C/min at 67 °C, a clearer first-order transition from the 2D Φ_h^{io} phase to the 3D $\Phi_{s\text{-}o}^{k}$ phase is detected (Figure 2). This transition is not observed on cooling with 10 °C/min (Figure 1). At −22 °C, an additional transition from the 3D $\Phi_{s\text{-}o}^{k}$ phase to a second 3D $\Phi_{s\text{-}o,1}^{k}$ phase is observed on cooling with 1 °C/min (Figure 2), while on cooling with 10 °C/min at −23 °C the 2D Φ_h^{io} transforms into the 3D Φ_h^{k} (Figure 1). On second heating scan with 1 °C/min, the 3D $\Phi_{s\text{-}o,1}^{k}$ phase transforms into the 3D $\Phi_{s\text{-}o}^{k}$ phase at −20 °C, while at 85 °C a more distinct first-order phase transition transforms the 3D $\Phi_{s\text{-}o}^{k}$ phase into the 2D Φ_h^{io} phase (Figure 2). The conclusion of this analysis is the following. At high temperature, the thermodynamic product of this assembly is the 2D Φ_h^{io} phase. At low temperature, the thermodynamic product is the 3D $\Phi_{s\text{-}o}^{k}$ phase. However, this product can be obtained only with cooling of 1 °C/min. With 10 °C/min at low temperature we can detect only the 2D Φ_h^{io} phase, which is the kinetic product of this assembly. The research hypothesis set at the start of this work asked the following question. Can small chemical modifications of the dendronized PBI transform its DSC scans recorded with 10 °C/min to look like the DSC scan of this sample recorded with 1 °C/min? Or, in other words, can we increase, by simple chemical modification, the rate of formation of the 3D $\Phi_{s\text{-}o}^{k}$ thermodynamic product from low temperature sufficiently to be detected by DSC scans recorded with 10 °C/min?

To answer this question, we will first discuss the DSC traces recorded with 1 °C/min for all dendronized PBIs with $n = 14-4$ from Figure 1. The $\Phi_h^{io}-i$ transition temperature from the first and second heating scans and the $i-\Phi_h^{io}$ from the first cooling

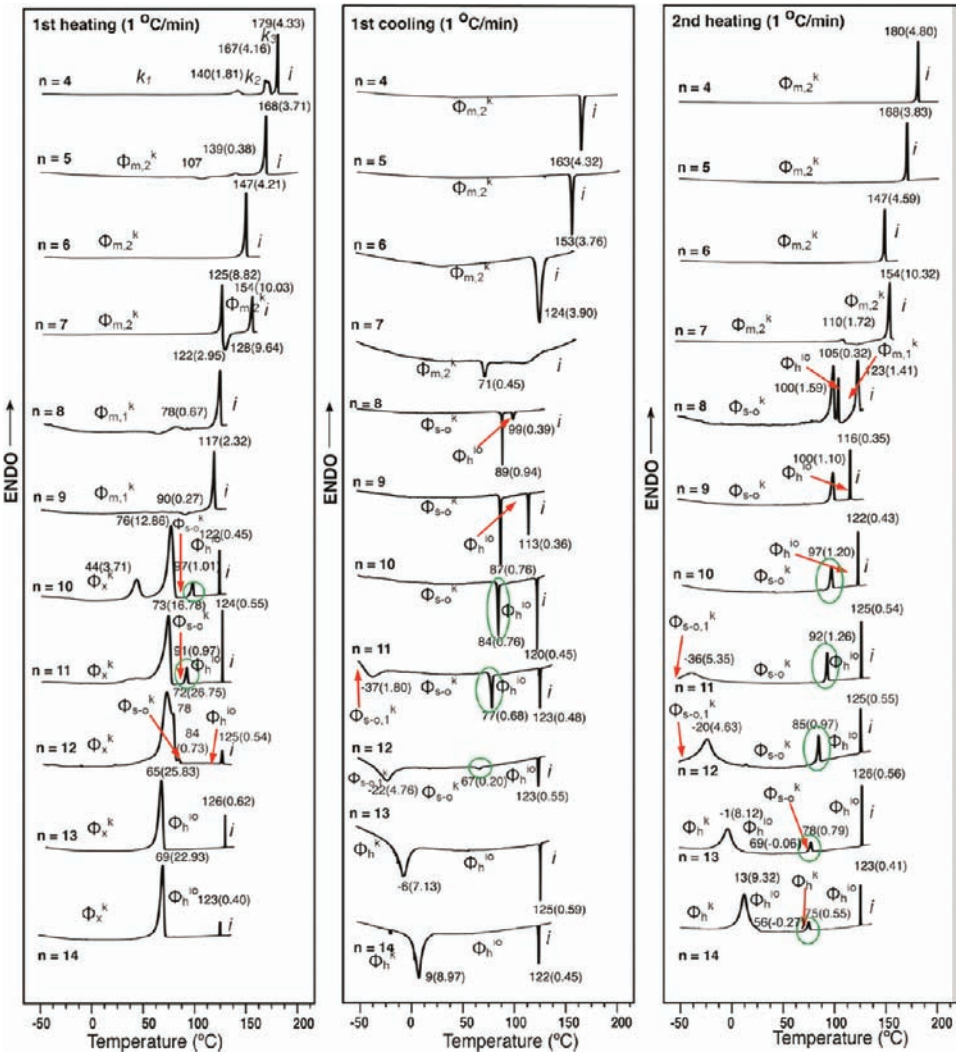

Figure 2. DSC traces of (3,4,5)*n*G1-3-PBI with $n = 14-4$ recorded with heating and cooling rates of 1 °C/min. Phases, transition temperatures, and associated enthalpy changes (in brackets in kcal/mol) are indicated. The green circles mark the transitions dependent on rate.

scan for compounds with $n = 14-8$ demonstrate that the Φ_h^{io} is thermodynamically stable and that this phase transition is thermodynamically controlled. This is demonstrated by the very small difference between this transition temperature and its enthalpy change observed on heating and cooling scans (Figures 1 and 2). At the same time, this transition temperature and its enthalpy change increase from $n = 8$ to $n = 13$, and subsequently both decrease at $n = 14$. The $\Phi_h^{io}-\Phi_{s\text{-}o}^{k}$ transition temperature from the second heating scan decreases from 105 °C for $n = 8$ to 75 °C for $n = 14$. At the same time, the corresponding enthalpy change increases from 0.32 kcal/mol at $n = 8$ to 1.26 kcal/mol at $n = 11$ and subsequently decreases to 0.56 kcal/mol at $n = 14$. On the first cooling scan, the degree of supercooling of the $\Phi_h^{io}-\Phi_{s\text{-}o}^{k}$ transition decreases from 5 °C for $n = 8$ to 18 °C for $n = 12$. No transition temperature change is observed for $n = 13$ and 14. The enthalpy change of this transition decreases continuously from 0.94 kcal/mol at $n = 8$ to 0.26 kcal/mol at $n = 12$. It is expected that subsequent decrease of this temperature for $n = 13$ and 14 brings it in the range of values overlapping the glass transition temperature, and, therefore, this phase transition becomes kinetically prohibited at $n = 13$ and 14. As a consequence, the $\Phi_{s\text{-}o}^{k}$ phase does not form for $n = 13$ and 14. The degree of supercooling of this temperature transition demonstrates that, although the $\Phi_{s\text{-}o}^{k}$ phase is the thermodynamic product at low temperature, its formation is kinetically controlled. As a consequence, even with cooling rates of 1 °C/min for $n = 13$ and 14, the thermodynamic product from low temperature does not form. During the first cooling and second heating scans, an additional crystal phase is formed between −37 and 9 °C on cooling, and −36 and 13 °C on heating for $n = 11-14$. This crystal phase maintains the symmetry of the next higher temperature phase and is most probably mediated by the crystallization tendency of the alkyl groups of the dendron. During the first heating scans, $n = 10-14$ exhibit at low temperature an unidentified crystal phase that, with the exception of $n = 10$ and 11, overlaps the $\Phi_{s\text{-}o}^{k}$ to Φ_h^{io} transition. The expected trend generated by the increase of the rate of heating and cooling from 1 °C/min to 10 °C/min is a decrease of all temperature transitions and of their enthalpy change and an enhancement of the degree of supercooling that is more substantial for kinetically controlled phase transitions. As a consequence, the Φ_h^{io} to $\Phi_{s\text{-}o}^{k}$ phase transition is not observed with rates of 10 °C/min for any of the dendronized PBIs with $n = 12-14$ and on heating only for $n = 11-8$. However, for $n = 8$, 9, 10, and 11,

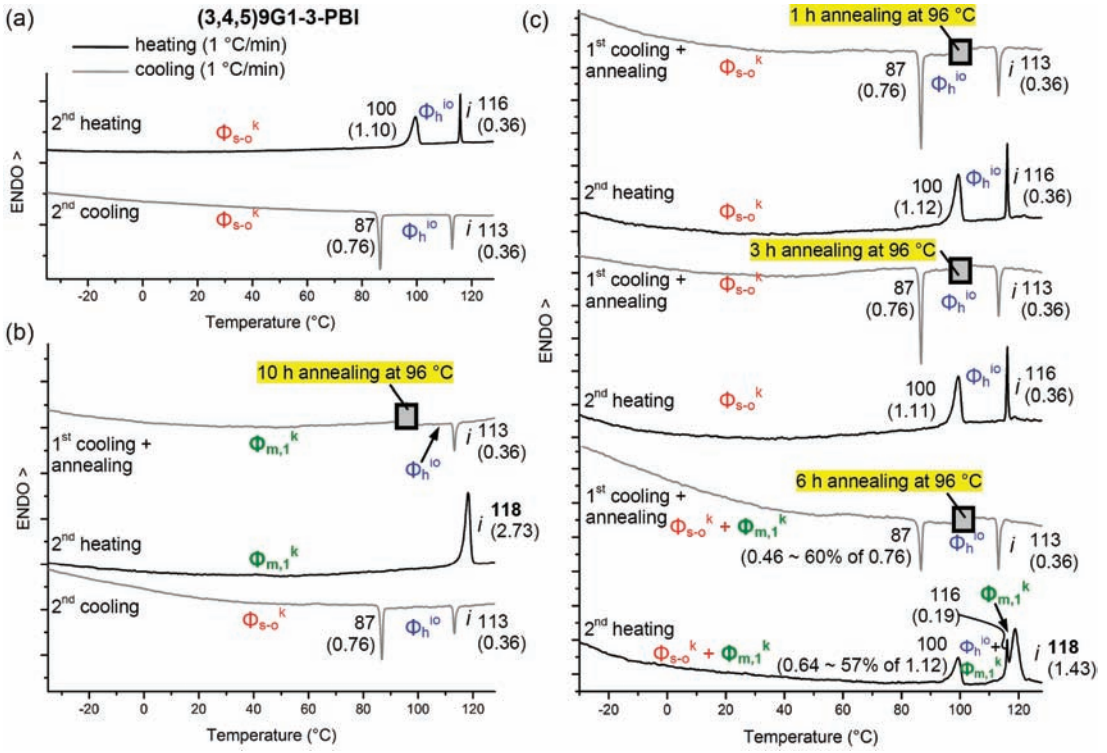

Figure 3. DSC traces collected with heating and cooling rates of 1 °C/min from (3,4,5)9G1-3-PBI. Second heating and cooling traces (a); first cooling to 96 °C, followed by 10 h annealing at 96 °C in the Φ_h^{io} phase, and the subsequent first and second heating and cooling traces (b); first cooling to 96 °C, followed by 1, 3, and 6 h annealing at 96 °C in the Φ_h^{io} phase, and the subsequent second heating (c). The data from (b) and (c) illustrate the complete and, respectively, partial transformation of the Φ_h^{io} phase into Φ_m^k crystal after annealing.

the formation of the $\Phi_{s\text{-}o}^k$ is observed with rates of both 1 and 10 °C/min. This is a very rewarding result because for n values from 11 to 8, the $\Phi_h^{io}-\Phi_{s\text{-}o}^k$ phase transition starts to transform from a kinetically controlled to a thermodynamically controlled. However, this remarkable change facilitates an even more important discovery that will be discussed with the help of the DSC experiments from Figure 3.

Figure 3a shows the second heating and cooling DSC scans of (3,4,5)9G1-3-PBI recorded with 1 °C/min. These scans are quite similar to the second heating and first cooling recorded with 1 °C/min (Figure 2) and 10 °C/min (Figure 1). Figure 3b shows the first cooling after annealing for 10 h at 96 °C in the Φ_h^{io} phase. Surprisingly, no $\Phi_{s\text{-}o}^k$ phase is observed upon cooling after this annealing process. Instead, a new monoclinic columnar crystal phase is observed ($\Phi_{m,1}^k$). In this new crystal phase, the self-repairing[13f] of the middle column from Scheme 1 takes place to generate the new column from the right side of the same scheme. This process will be discussed in more detail in a later subsection. The second heating scan after cooling shows only the $\Phi_{m,1}^k$ phase that undergoes melting directly to an isotropic phase at 118 °C. Cooling from the isotropic melt regenerates a second cooling DSC scan that is identical to the first cooling scan from Figure 2. This result also demonstrates that this compound does not undergo thermal decomposition during 10 h annealing at high temperature followed by slow cooling and reheating cycles. Figure 3c investigates the role of the annealing time at 96 °C on the formation of the new $\Phi_{m,1}^k$ phase. Cooling scans followed by second heating scans after annealing for 1 and 3 h at 96 °C are not sufficient to generate the $\Phi_{m,1}^k$ phase. After 6 h of annealing at 96 °C, a mixture of $\Phi_{s\text{-}o}^k$ and $\Phi_{m,1}^k$ phases is formed, which upon second heating displays a mixture of $\Phi_{s\text{-}o}^k$, $\Phi_{m,1}^k$ transforming into a mixture of Φ_h^{io} and $\Phi_{m,1}^k$ that at 116 °C generates only the $\Phi_{m,1}^k$ phase, which undergoes melting to an isotropic liquid at 118 °C.

At this point, we can reinvestigate the DSC traces of (3,4,5)-8G1-3-PBI recorded with 1 °C/min from Figure 2. The second heating scan of (3,4,5)8G1-3-PBI from Figure 2 resembles the sequence of phases displayed by the second heating of (3,4,5)9G1-3-PBI after annealing for 6 h at 96 °C (Figure 3c). It displays the sequence $\Phi_{s\text{-}o}^k$, which transforms at 100 °C into Φ_h^{io} that undergoes isotropization at 105 °C and immediate crystallization through an exothermic peak that overlaps with the formation of the $\Phi_{m,1}^k$ phase. The $\Phi_{m,1}^k$ phase melts into an isotropic liquid at 123 °C. During the first heating scans, both n = 8 and 9 display only the $\Phi_{m,1}^k$ phase that exhibits a much lower degree of perfection than the one obtained after annealing in the Φ_h^{io} phase. The main message of these experiments is that the thermodynamic product for n = 8 and 9 is not the $\Phi_{s\text{-}o}^k$ but the newly discovered and more ordered $\Phi_{m,1}^k$ phase. However, the formation of the $\Phi_{m,1}^k$ phase is kinetically controlled and forms very slowly only upon proper annealing in the Φ_h^{io} phase.

Regardless of the heating and cooling rates, the dendronized PBIs with n = 7−4 display only an additional monoclinic crystal ($\Phi_{m,2}^k$) that was not yet elucidated (Figures 1 and 2). The results of the DSC analysis combined with the phase assignments established by XRD are summarized in Table 1. The detailed analysis of these supramolecular assemblies by a combination of small-angle (SAXS) and wide-angle (WAXS) XRD experiments will be presented in the following sections.

Structural Analysis of the Library of Dendronized PBIs by SAXS and WAXS. The phases reported in Tables 1 and 2 and in

Table 1. Transition Temperatures and Associated Enthalpy Changes of (3,4,5)*n*G1-3-PBI with *n* = 4−14 As Determined by DSC and XRD

		thermal transitions (°C) and corresponding enthalpy changes (kcal/mol)	
n	rate (°C/min)	heating[a]	cooling
4	10	k_1 133 (0.64) k_2 141 (4.13) k_3 180 (4.84) i $\Phi_{m,2}{}^{k}$ 179 (4.95) i	i 143 (3.74) $\Phi_{m,2}{}^{k}$
	1	k_1 140 (1.81) k_2 167 (4.16) k_3 179 (4.33) i $\Phi_{m,2}{}^{k}$ 180 (4.80) i	i 163 (4.32) $\Phi_{m,2}{}^{k}$
5	10	$\Phi_{m,2}{}^{k}$ 167 (3.78) i $\Phi_{m,2}{}^{k}$ 167 (4.36) i	i 142 (3.89) $\Phi_{m,2}{}^{k}$
	1	$\Phi_{m,2}{}^{k}$ 139 (0.38) $\Phi_{m,2}{}^{k}$ 168 (3.71) i $\Phi_{m,2}{}^{k}$ 168 (3.83) i	i 153 (3.76) $\Phi_{m,2}{}^{k}$
6	10	$\Phi_{m,2}{}^{k}$ 147 (4.03) i $\Phi_{m,2}{}^{k}$ 86 (0.6) $\Phi_{m,2}{}^{k}$ 147 (3.88) i	i 114 (1.17) $\Phi_{m,2}{}^{k}$
	1	$\Phi_{m,2}{}^{k}$ 147 (4.21) i $\Phi_{m,2}{}^{k}$ 147 (4.59) i	i 124 (3.90) $\Phi_{m,2}{}^{k}$
7	10	$\Phi_{m,2}{}^{k}$ 126 (10.76) i $\Phi_{m,2}{}^{k}$ 77 (0.71) $\Phi_{m,2}{}^{k}$ 110 (1.34) i	i −[b] $\Phi_{m,2}{}^{k}$
	1	$\Phi_{m,2}{}^{k}$ 125 (8.82) $\Phi_{m,2}{}^{k}$ 154 (10.03) i $\Phi_{m,2}{}^{k}$ 110 (1.72) $\Phi_{m,2}{}^{k}$ 154 (10.32) i	i 71 (0.45) $\Phi_{m,2}{}^{k}$
8	10	$\Phi_{m,1}{}^{k}$ 121 (2.59) i $\Phi_{s\text{-}o}{}^{k}$ 91 (0.33) −[c] 98 (0.26) −[c] 104 (0.30) i	i 85 (0.62) $\Phi_{h}{}^{io}$ 80 (0.40) $\Phi_{s\text{-}o}{}^{k}$
	1	$\Phi_{m,1}{}^{k}$ 78 (0.67) $\Phi_{m,1}{}^{k}$ 122 (2.95) i $\Phi_{s\text{-}o}{}^{k}$ 100 (1.59) $\Phi_{h}{}^{io}$ 105 (0.32) $\Phi_{m,1}{}^{k}$ 123 (1.41) i	i 99 (0.39) $\Phi_{h}{}^{io}$ 89 (0.94) $\Phi_{s\text{-}o}{}^{k}$
9	10	$\Phi_{m,1}{}^{k}$ 116 (2.51) i $\Phi_{s\text{-}o}{}^{k}$ 85 (0.12) $\Phi_{s\text{-}o}{}^{k}$ 96 (1.14) $\Phi_{h}{}^{io}$ 116 (0.44) i	i 108 (0.41) $\Phi_{h}{}^{io}$ 83 (0.58) $\Phi_{s\text{-}o}{}^{k}$
	1	$\Phi_{m,1}{}^{k}$ 90 (0.27) $\Phi_{m,1}{}^{k}$ 117 (2.32) i $\Phi_{s\text{-}o}{}^{k}$ 100 (1.10) $\Phi_{h}{}^{io}$ 116 (0.35) i $\Phi_{m,1}{}^{k}$ 118 (2.73) i[d]	i 113 (0.36) $\Phi_{h}{}^{io}$ 87 (0.76) $\Phi_{s\text{-}o}{}^{k}$
10	10	$\Phi_{x}{}^{k}$ 81 (14.18) $\Phi_{s\text{-}o}{}^{k}$ 96 (0.73) $\Phi_{h}{}^{io}$ 122 (0.50) i $\Phi_{s\text{-}o}{}^{k}$ 97 (1.05) $\Phi_{h}{}^{io}$ 123 (0.51) i	i 118 (0.45) $\Phi_{h}{}^{io}$ 80 (0.49) $\Phi_{s\text{-}o}{}^{k}$
	1	$\Phi_{x}{}^{k}$ 76 (12.86) $\Phi_{s\text{-}o}{}^{k}$ 97 (1.01) $\Phi_{h}{}^{io}$ 122 (0.45) i $\Phi_{s\text{-}o}{}^{k}$ 97 (1.20) $\Phi_{h}{}^{io}$ 122 (0.43) i	i 120 (0.45) $\Phi_{h}{}^{io}$ 84 (0.76) $\Phi_{s\text{-}o}{}^{k}$
11	10	$\Phi_{x}{}^{k}$ 76 (18.08) $\Phi_{s\text{-}o}{}^{k}$ 90 (0.48) $\Phi_{h}{}^{io}$ 124 (0.50) i $\Phi_{s\text{-}o}{}^{k}$ 91 (1.03) $\Phi_{h}{}^{io}$ 124 (0.54) i	i 120 (0.50) $\Phi_{h}{}^{io}$ 70 (0.27) $\Phi_{s\text{-}o}{}^{k}$
	1	$\Phi_{x}{}^{k}$ 73 (16.78) $\Phi_{s\text{-}o}{}^{k}$ 91 (0.97) $\Phi_{h}{}^{io}$ 124 (0.55) i $\Phi_{s\text{-}o,1}{}^{k}$ −36 (5.35) $\Phi_{s\text{-}o}{}^{k}$ 92 (1.26) $\Phi_{h}{}^{io}$ 125 (0.54) i	i 123 (0.48) $\Phi_{h}{}^{io}$ 77 (0.68) $\Phi_{s\text{-}o}{}^{k}$ −37 (1.80) $\Phi_{s\text{-}o,1}{}^{k}$
12	10	$\Phi_{x}{}^{k}$ 80 (28.91) $\Phi_{h}{}^{io}$ 125 (0.55) i $\Phi_{h}{}^{k}$ −17 (4.44) $\Phi_{h}{}^{io}$ 73 (−0.25) $\Phi_{s\text{-}o}{}^{k}$ 84 (0.86) $\Phi_{h}{}^{io}$ 125 (0.59) i	i 121 (0.62) $\Phi_{h}{}^{io}$ −23 (3.96) $\Phi_{h}{}^{k}$
	1	$\Phi_{x}{}^{k}$ 72 (26.75) $\Phi_{s\text{-}o}{}^{k}$ 84 (0.73) $\Phi_{h}{}^{io}$ 125 (0.54) i $\Phi_{s\text{-}o,1}{}^{k}$ −20 (4.63) $\Phi_{s\text{-}o}{}^{k}$ 85 (0.97) $\Phi_{h}{}^{io}$ 125 (0.55) i	i 123 (0.55) $\Phi_{h}{}^{io}$ 67 (0.20) $\Phi_{s\text{-}o}{}^{k}$ −22 (4.76) $\Phi_{s\text{-}o,1}{}^{k}$
13	10	$\Phi_{x}{}^{k}$ 69 (29.9) $\Phi_{h}{}^{io}$ 126 (0.68) i $\Phi_{h}{}^{k}$ 0 (10.44) $\Phi_{h}{}^{io}$ 126 (0.69) i	i 123 (0.69) $\Phi_{h}{}^{io}$ −5 (10.32) $\Phi_{h}{}^{k}$
	1	$\Phi_{x}{}^{k}$ 65 (25.83) $\Phi_{h}{}^{io}$ 126 (0.62) i $\Phi_{h}{}^{k}$ −1 (8.12) $\Phi_{h}{}^{io}$ 69 (−0.06) $\Phi_{s\text{-}o}{}^{k}$ 78 (0.79) $\Phi_{h}{}^{io}$ 126 (0.56) i	i 125 (0.59) $\Phi_{h}{}^{io}$ −6 (7.13) $\Phi_{h}{}^{k}$
14	10	$\Phi_{x}{}^{k}$ 75 (16.07) $\Phi_{h}{}^{io}$ 121 (0.73) i $\Phi_{h}{}^{k}$ 15 (11.59) $\Phi_{h}{}^{io}$ 121 (0.43) i	i 117 (0.55) $\Phi_{h}{}^{io}$ 8 (12.21) $\Phi_{h}{}^{k}$
	1	$\Phi_{x}{}^{k}$ 69 (22.93) $\Phi_{h}{}^{io}$ 123 (0.40) i $\Phi_{h}{}^{k}$ 13 (9.32) $\Phi_{h}{}^{io}$ 56 (−0.27) $\Phi_{h}{}^{k}$ 75 (0.55) $\Phi_{h}{}^{io}$ 123 (0.41) i	i 122 (0.45) $\Phi_{h}{}^{io}$ 9 (8.97) $\Phi_{h}{}^{k}$

[a] First heating data on the first line and second heating data on the second line. [b] Transition observed by XRD. [c] Phases could be resolved only in the XRD experiments performed with 1 °C/min. [d] Second heating DSC data collected after annealing for 10 h at 96 °C followed by cooling to −40 °C with a rate of 1 °C/min. Note: Quantitative uncertainties are ±1 °C for thermal transition temperatures and ∼2% for the associated enthalpy changes reported in kcal/mol.

Figures 1, 2, and 3 were assigned by the analysis of SAXS and WAXS powder and oriented fiber XRD data recorded as a function of temperature. To match the experimental conditions used in the DSC experiments, these XRD experiments were

Table 2. Structural Analysis of (3,4,5)*n*G1-3-PBI with *n* = 4−14 by XRD

n	*T* (°C)	phase[a]	*a*, *b*, *c* (Å)[b]	*α*, *β*, *γ* (deg)[b]	*μ*[c]	experimental *d*-spacings (Å)
14	35	Φ_x^{kp}	103.0, 65.0			−, 55.1, 25.7, 21.2, 18.3, 17.2, 16.3[d]
	120	Φ_h^{io}	41.7		2	36.1, 20.8, 18.0[f]
	30	Φ_h^{k}	46.8, −, 60.5		2	40.5, 23.4, 20.3, −, 33.7[e]
	−40	Φ_h^{k}	45.7, −, 60.1		2	39.7, 22.9, 19.8, −, 33.1[e]
13	50	Φ_x^{kp}	105.9, 40.6			53.1, 37.9, −, −, −, 17.7, 16.1[d]
	75	$\Phi_{s\text{-}o}^{k}$	76.8, 45.0, 58.2		2	−, 38.8, 38.4, 35.6, 32.3, 32.1, 29.1, 29.2, 26.1, 23.3[g]
						22.5, 20.6, 21.6, 20.8, 17.8, 19.2, 17.4, 17.3, 18.2, 17.3, 16.2[h]
	110	Φ_h^{io}	40.9		2	35.5, 20.5, 17.7[f]
	−25	Φ_h^{k}	43.7		2	37.9, 21.9, 18.9[f]
12	20	Φ_x^{kp}	76.9, 71.8			52.6, 33.9, 23.9, 20.9, 20.5, 17.0[i]
	80	$\Phi_{s\text{-}o}^{k}$	74.4, 43.2, 60.6		2	60.6, 37.4, 37.2, 35.2, 31.8, 31.7, 30.3, 28.2, 25.6, 23.5[g]
						21.6, 20.6, 20.7, −, 18.3, 18.6, 17.8, 17.7, −, −, 16.4[h]
	110	Φ_h^{io}	40.0		2	34.7, 20.0, 17.3[f]
11	90	$\Phi_{s\text{-}o}^{k}$	71.5, 42.2, 60.6		2	60.6, 36.3, 35.8, 34.6, 31.2, 30.8, 30.3, 27.3, 24.9, 23.3[g]
						21.1, 20.3, 20.2, 19.6, 18.2, 17.9, 17.7, 17.6, 17.1, 16.8, 16.2[h]
	110	Φ_h^{io}	39.2		2	33.9, −, −[f]
10	80	$\Phi_{s\text{-}o}^{k}$	69.0, 40.7, 60.4		2	−, 35.1, 34.5, 33.8, 30.3, 29.9, 30.2, 26.3, 24.1, 22.9[g]
						20.4, 19.8, 19.5, 19.0, 18.1, 17.3, 17.5, 17.4, 16.6, 16.4, 16.0[h]
	105	Φ_h^{io}	38.0		2	32.9, −, −[f]
9	25	$\Phi_{m,1}^{k}$	76.0, 76.8, 28.8	90, 102.0, 90	2	74.3, 37.2, 33.5, −, 26.7, 26.5, 24.7, 23.9, 23.5, 19.8, 19.0, −[j]
						−, 18.9, 18.4, 17.9, −, 17.3, 16.8, −, 16.5, 16.2, 16.0, 14.4, −[k]
	90	$\Phi_{s\text{-}o}^{k}$	67.3, 39.6, 60.8		2	−, 34.1, 33.7, 33.2, 29.8, 29.5, 30.4, 25.6, 23.6, 22.7[g]
						19.8, 19.6, 19.0, 18.6, 18.1, 16.8, 17.4, 17.3, 16.2, 16.1, 15.9[h]
	110	Φ_h^{io}	37.5		2	32.5, −, −[f]
8	80	$\Phi_{s\text{-}o}^{k}$	65.0, 38.2, 60.5		2	−, 32.9, 32.5, 32.3, 28.9, 28.6, 30.3, 24.8, 22.9, 22.3[g]
						19.1, 19.2, 18.3, 18.0, 17.8, 16.3, 17.2, 17.1, 15.7, 15.6, 15.6[h]
	100	Φ_h^{io}	36.7		2	31.9, −, −[f]
	120	$\Phi_{m,1}^{k}$	72.5, 79.9, 29.7	90, 101.4, 90	2	−, 35.5, −, 27.3, 26.5, 27.4, −, 23.9, 24.1, 19.9, −, 23.5[j]
						20.6, −, 18.2, −, 17.8, 16.7, −, 13.8, −, −, −, 14.9, 13.5[k]
7	25	$\Phi_{m,2}^{k}$	29.4, 18.3, 15.4	90, 90, 103.5		28.6, 15.4, 11.6, 10.2, 9.5, 8.5, 8.4[l]
6	25	$\Phi_{m,2}^{k}$	38.5, 44.2, 34.0	90, 90, 95.6		38.3, 25.4, 22.0, 19.9, 13.5, 12.8, 11.5, 10.9, 8.5, 8.4, 8.1, 7.1[m]
5	25	$\Phi_{m,2}^{k}$	71.7, 33.6, 45.1	90, 90, 109.0		35.9, 24.9, 22.6, 21.3, 19.3, 18.7[n]
4	25	$\Phi_{m,2}^{k}$	34.8, 27.8, 28.4	90, 90, 94.8		34.8, 28.4, 27.8, 22.1, 20.9, 19.5, 16.7, 13.9, 12.3, 10.5, 10.0, 9.2, 8.7, 8.3[o]

[a] Φ_h^{k}: Columnar hexagonal crystalline phase. Φ_m^{k}: Monoclinic columnar crystalline phase. Φ_x^{k}: Unidentified columnar crystalline phase. Φ_h^{io}: Columnar hexagonal phase with intracolumnar order. $\Phi_{s\text{-}o}^{k}$: Simple orthorhombic columnar crystalline phase. [b] Lattice parameters (with uncertainty of ∼1%) calculated using: $d_{hkl} = [4(h^2 + k^2 + hk)/(3a^2) + (l/c)^2]^{-1/2}$ for hexagonal, $d_{hk} = [(h/a)^2 + (k/b)^2]^{-1/2}$ for the indexing of the equatorial peaks of Φ_x^{k}, $d_{hkl} = [(h/a)^2 + (k/b)^2 + (l/c)^2]^{-1/2}$ for orthorhombic lattices, and $d_{hkl} = [(h/a \sin\gamma)^2 + (k/b \sin\gamma)^2 + (l/c)^2 - (2hk \cos\gamma/ab \sin^2\gamma)]^{-1/2}$ or $d_{hkl} = [(h/a \sin\beta)^2 + (k/b)^2 + (l/c \sin\beta)^2 - (2hl \cos\beta/ac \sin^2\beta)]^{-1/2}$ for monoclinic phases. [c] Average number of dendrimers forming the supramolecular column stratum with thickness t = 3.7 Å, calculated using: $\mu = N_A abt\rho/(2M_{wt})$. $N_A = 6.022 \times 10^{23}$ mol^{-1} = Avogadro's number. ρ = 1.05 g/cm^3 and M_{wt} are the density and molecular weight. [d] d_{20}, d_{11}, d_{40}, d_{13}, d_{33}, d_{60}, d_{04}. [e] d_{100}, d_{110}, d_{200}, d_{210}, d_{101}. [f] d_{10}, d_{11}, d_{20}. [g] d_{001}, d_{110}, d_{200}, d_{011}, d_{111}, d_{201}, d_{002}, d_{210}, d_{211}, d_{112}. [h] d_{020}, d_{212}, d_{120}, d_{311}, d_{013}, d_{400}, d_{113}, d_{203}, d_{401}, d_{122}, d_{213}. [i] d_{11}, d_{21}, d_{03}, d_{32}, d_{42}, d_{51}. [j] d_{100}, d_{200}, d_{210}, d_{111}, d_{220}, d_{011}, $d_{10\bar{1}}$, d_{211}, $d_{11\bar{1}}$, $d_{21\bar{1}}$, d_{131}, d_{121}. [k] $d_{20\bar{1}}$, d_{031}, d_{321}, d_{231}, d_{400}, d_{401}, d_{411}, $d_{41\bar{1}}$, $d_{31\bar{1}}$, d_{331}, $d_{23\bar{1}}$, d_{102}, $d_{11\bar{2}}$. [l] d_{100}, d_{001}, d_{011}, $d_{1\bar{1}1}$, d_{300}, d_{220}, $d_{2\bar{1}1}$. [m] d_{100}, d_{101}, d_{020}, d_{120}, d_{031}, d_{300}, d_{320}, d_{321}, d_{051}, d_{341}, d_{251}, d_{530}. [n] d_{200}, $d_{2\bar{1}1}$, d_{002}, d_{301}, d_{211}, d_{012}. [o] d_{100}, d_{001}, d_{010}, d_{101}, d_{110}, d_{011}, d_{111}, d_{020}, d_{021}, d_{220}, $d_{\bar{3}11}$, d_{030}, d_{320}, d_{321}. [p] Phase observed only in the first heating of the as-prepared compound.

performed with heating and cooling rates ranging from 1 to 10 °C/min.

The structural analysis of the periodic arrays self-organized by the library (3,4,5)*n*G1-3-PBI will be discussed starting from *n* = 4 to *n* = 14 (Figure 4). The diversity of lattices observed for the dendronized PBIs indicates the significant contribution of *n* on their self-assembly (Table 1, Figure 4). For the current discussion, the library of dendronized PBIs was organized into the following four sublibraries: *n* = 4, 5, 6, 7; *n* = 8, 9; *n* = 10, 11, 12; and *n* = 13, 14. The dendronized PBIs with *n* = 4−7 self-organize into a variety of monoclinic crystalline ($\Phi_{m,2}^{k}$) phases characterized by a *c*-axis ranging from 15.4 Å for *n* = 7 to 45.1 Å for *n* = 5. The WAXS fiber patterns of the $\Phi_{m,2}^{k}$ phases observed in *n* = 4−7 (Figure 4) exhibit sharp off-meridional wide-angle features in the range of 3.5−4.1 Å. These features, in combination with the absence of meridian diffraction peaks in the range expected for the *π*−*π* stacking corresponding to a distance of ∼3.5 Å, suggest that, most probably, the dendronized PBIs are tilted with respect to the long axis of the supramolecular column. A tilted organization of the dendronized PBIs can also explain the

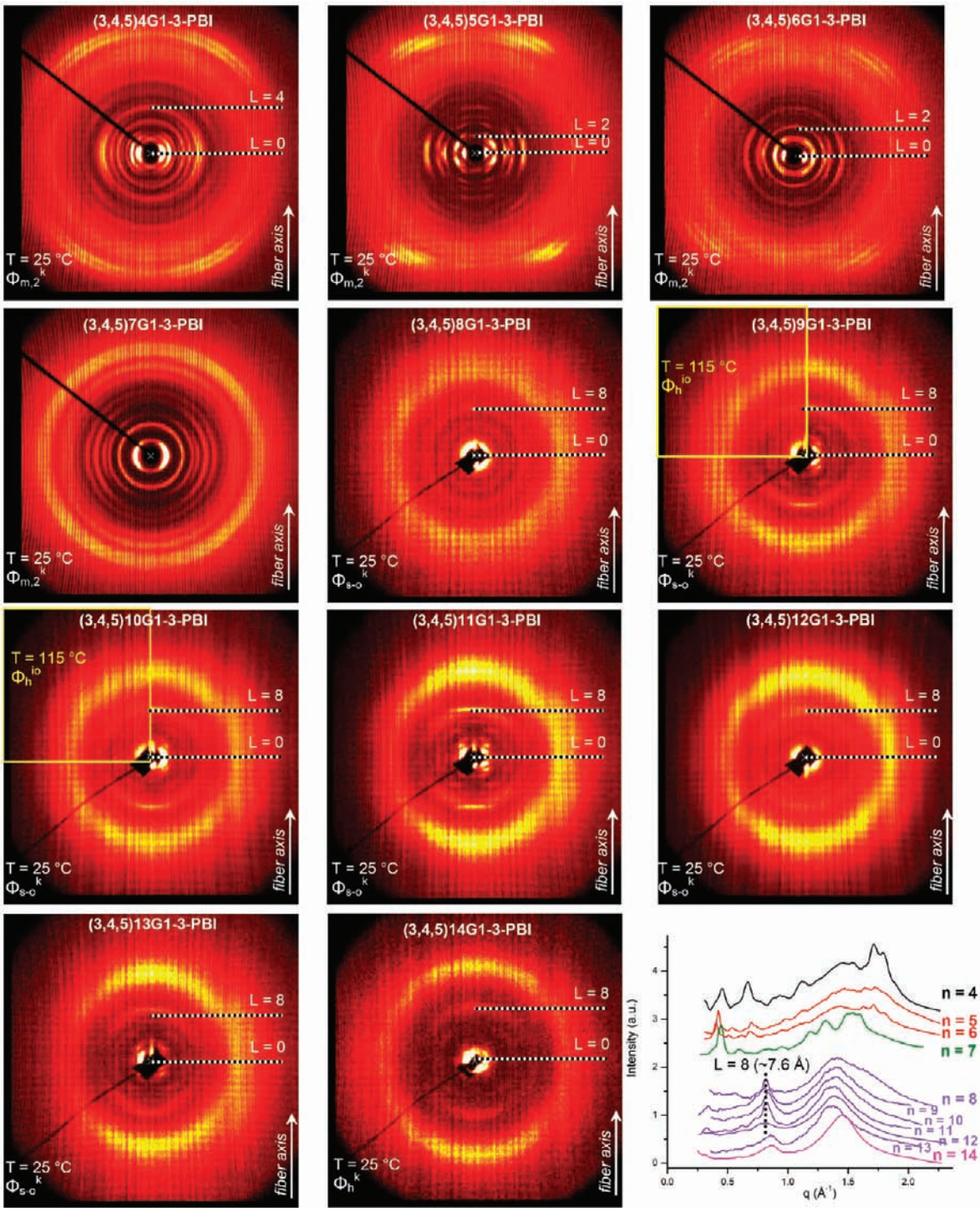

Figure 4. The wide-angle X-ray patterns collected from the oriented samples of (3,4,5)*n*G1-3-PBI, with n = 4−14, and the corresponding meridional plots.

significant variation of the lattice parameters of the $\Phi_{m,2}^{k}$ phases upon the increase of n from 4 to 7 (Table 2).

The second sublibrary of dendronized PBIs, n = 8, 9, exhibits the 3D $\Phi_{s\text{-}o}^{k}$, the 3D $\Phi_{m,1}^{k}$, and the 2D Φ_{h}^{io} phases. This latter result demonstrates that the increase of the conformational freedom of the dendronized PBI induced by the transition of n from 7 to 8 and to 9 is responsible for the creation of the Φ_{h}^{io} phase in addition to the low-temperature crystalline phases observed in all compounds with n < 8. The WAXS fiber patterns collected in the low temperature range of $\Phi_{s\text{-}o}^{k}$ and in the high temperature of Φ_{h}^{io} phases (Figure 4) exhibit equatorial features at ~7.6 Å. These equatorial reflections are due to the thickness of the supramolecular tetramers of 7.6 Å generated by a pair of side-by-side dendronized PBIs arranged on top of a second pair of side-by-side dendronized PBI and rotated at a certain angle (Scheme 1). This arrangement is similar to that observed in the

dx.doi.org/10.1021/ja208501d |*J. Am. Chem. Soc.* 2011, 133, 18479–18494

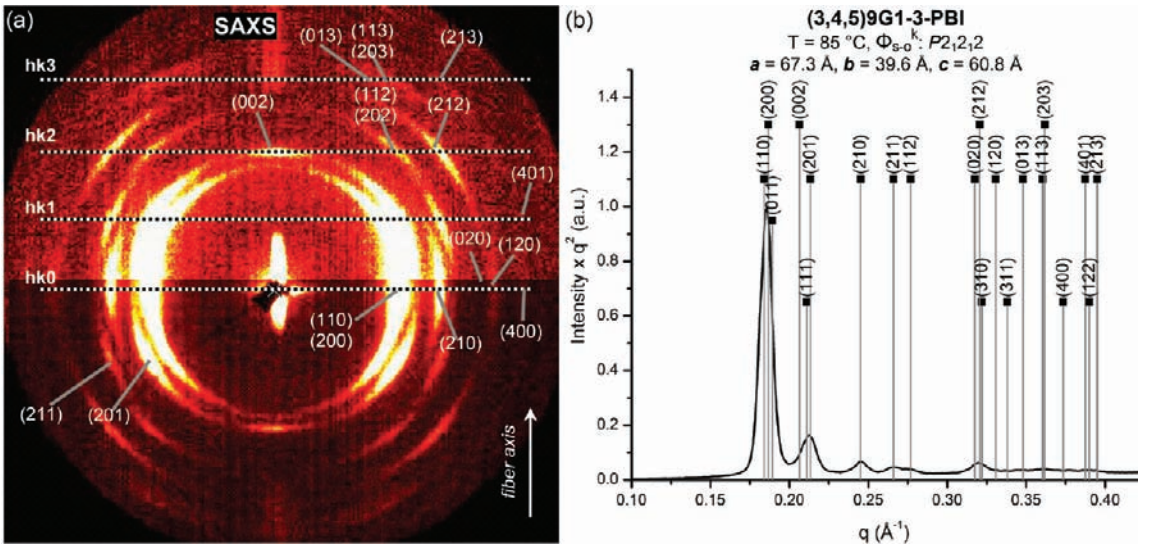

Figure 5. The SAXS fiber pattern collected at 85 °C from the oriented fiber of (3,4,5)9G1-3-PBI (a), and the corresponding plot (b). Fiber axis, diffraction peaks, indexing, and lattice parameters of the simple crystalline orthorhombic phase, $\Phi_{s\text{-}o}{}^{k}$, are indicated.

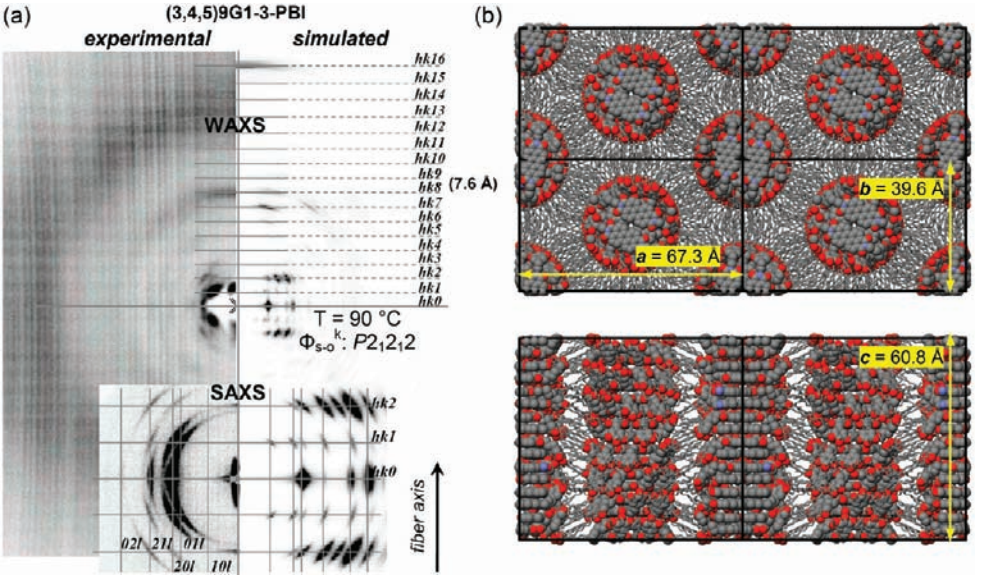

Figure 6. Comparison of the experimental and simulated fiber patterns of (3,4,5)9G1-3-PBI collected at 90 °C in the $\Phi_{s\text{-}o}{}^{k}$ phase (a) and the corresponding molecular model used in the simulation (b).

compound with $n = 12$ that was reported previously.[10] The SAXS fiber pattern collected from the oriented sample with $n = 9$ and its indexing to the $\Phi_{s\text{-}o}{}^{k}$ phase with $P2_12_12$ symmetry are shown in Figure 5. The SAXS fiber data collected in the $\Phi_{s\text{-}o}{}^{k}$ phases with $P2_12_12$ symmetry observed in the dendronized PBIs with $n = 8-13$ and their indexing are summarized in the Supporting Information. The simulation of the XRD fiber data collected in $\Phi_{s\text{-}o}{}^{k}$ phase of the dendronized PBI with $n = 9$ and the molecular model used in the simulation are outlined in Figure 6. As it was shown previously for the case of $n = 12$,[10] the analysis of the XRD data collected in the $\Phi_{s\text{-}o}{}^{k}$ and $\Phi_{h}{}^{io}$ phases and the simulation of the XRD fiber patterns (Figure 6) demonstrated that the columns forming these phases are generated via a helical arrangement of the supramolecular tetramers (Scheme 1). It is important to note that both in $\Phi_{s\text{-}o}{}^{k}$ and in $\Phi_{h}{}^{io}$ phases, assembled from the dendronized PBIs with $n = 8-14$, the aromatic core of the supramolecular columns is generated by pairs of PBIs that are arranged side-by-side and another pair in the next stratum of the column turned upside-down and rotated at a certain angle. The intratetramer stacking distance in the helical columns is 4.1 Å, while the intertetramer stacking distance is 3.5 Å (Scheme 1).

The $\Phi_{m,1}{}^{k}$ phases observed in the first heating of the $n = 8$ and 9 were also detected in the second heating with slow heating rate for $n = 8$ (Figure 2) or after annealing in the $\Phi_{h}{}^{io}$ phase for $n = 9$ (Figures 3 and 7). The XRD and electron diffraction (ED) data collected in the $\Phi_{m,1}{}^{k}$ phase of $n = 9$ (Table 1 and Figures 1, 2, 3, and 7) will be discussed in the following subsection.

The third sublibrary of dendronized PBIs, $n = 10$, 11, 12, exhibits at low temperatures the $\Phi_{s\text{-}o}{}^{k}$ phase with $P2_12_12$ symmetry[10]

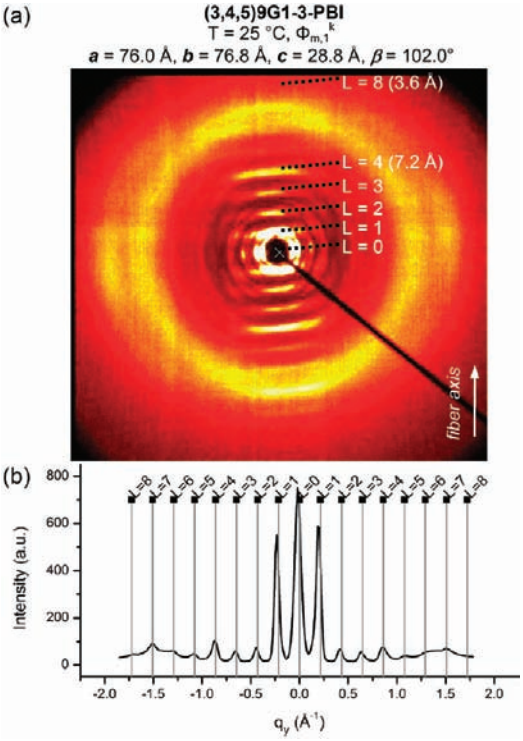

Figure 7. The WAXS fiber pattern collected from (3,4,5)9G1-3-PBI in the $\Phi_{m,1}^{k}$ phase obtained after annealing at 110 °C in the Φ_{h}^{io} phase for 10 h (see also Figure 3c) (a) and the corresponding q_y plot (b).

and at high temperatures the Φ_{h}^{io} phase (Figure 4). This sequence is similar to that of the phases observed for the second sublibrary n = 8, 9. In contrast to the structures with $n \leq 9$, the third sublibrary of dendronized PBIs does not exhibit the $\Phi_{m,1}^{k}$ phase. For example, in the case of n = 10, the XRD fiber pattern was unchanged even after annealing in the Φ_{h}^{io} phase at 115 °C (Figures 1 and 2) for more than 12 h. However, in the case of n = 9, some of the diffraction features corresponding to the $\Phi_{m,1}^{k}$ phase were observed after only 30 min of annealing at 110 °C. It is important to note that only in the narrow range for the structural parameter n of 8 and 9 does the self-organization process induce the highly ordered columns to self-repair and assemble into the $\Phi_{m,1}^{k}$ phase characterized by all side-by-side dendronized PBIs pairs stacked only at 3.5 Å (Figure 7). The fourth sublibrary of dendronized PBIs with n = 13 and 14 exhibits at low temperature a Φ_{h}^{k} phase and at high temperature the Φ_{h}^{io} (Figures 1, 2, and 4). The $\Phi_{s\text{-}o}^{k}$ phase with $P2_12_12$ symmetry was observed only for n = 13 at intermediate temperatures after second heating scans performed with rates of 1 °C/min or slower. In the case of n = 14, a Φ_{h}^{k} phase replaces the $\Phi_{s\text{-}o}^{k}$ phase observed for n = 13.

Structural Analysis of (3,4,5)9G1-3-PBI in the $\Phi_{m,1}^{k}$ Phase by a Combination of Electron Diffraction (ED) and XRD Experiments. Figure 8 shows the SAXS powder data collected for the dendronized PBI with n = 9 from the first heating of the as-prepared compound as well as from subsequent cooling and heating scans performed with 1 °C/min. After 10 h of annealing in the high temperature Φ_{h}^{io} phase, the $\Phi_{m,1}^{k}$ phase identified in the first heating scan of the as-prepared compound is recovered (Figures 8 and 9).

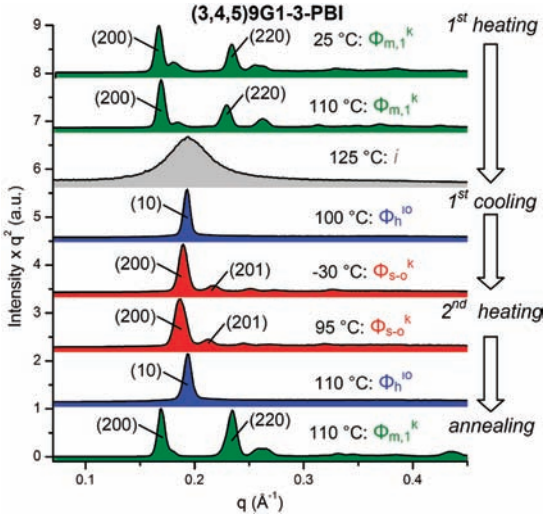

Figure 8. The SAXS powder data collected from (3,4,5)9G1-3-PBI at the indicated temperatures.

The transition from Φ_{h}^{io} to $\Phi_{m,1}^{k}$ was also monitored in the second heating scan of the oriented fibers of this compound (Figure 9). The experiments performed on oriented fibers are complementary to the powder XRD data and facilitated a separation of the diffraction features (*hk*0) and (*hkl*) from the SAXS region. This separation demonstrated that the Φ_{h}^{io} to $\Phi_{m,1}^{k}$ transition begins after ~30 min of annealing (Figure 9). On the other hand, the DSC experiments could detect significant enthalpy changes only following annealing for longer than 180 min (Figure 3). These results indicate that only a relative small fraction of the compound is transformed after 30 min of annealing. Considering that in the case of the n = 8 the structure of the $\Phi_{m,1}^{k}$ phase was observed to form in the second heating performed with rates of 1 °C/min, it is not surprising that for n = 9 the transformation Φ_{h}^{io} to $\Phi_{m,1}^{k}$ starts after ~30 min of annealing (Figures 2 and 9). However, this transformation was complete only after annealing for 600 min (Figures 3 and 9).

A similar annealing experiment was performed on a thin film prepared by casting a solution from n = 9 dissolved in THF, which was analyzed by electron diffraction. Figure 10 shows a series of electron diffraction patterns collected after annealing the thin film at 96 °C following slow cooling from the isotropic phase. The electron diffraction data showed that the *a* and *b* axes of the lattice are perpendicular to each other and that the *c*-axis is inclined by β = 102° with respect to the *a*,*b* plane. Therefore, the electron diffraction results are consistent with the $\Phi_{m,1}^{k}$ unit cell. The lattice parameters provided by the analysis of the electron diffraction data are in excellent agreement with those obtained from the XRD analysis. Furthermore, the same number of layers identified in the electron diffraction pattern shown in Figure 10c was also observed in the wide-angle XRD fiber pattern from Figure 10b.

Figure 11 compares the lattice parameters of the $\Phi_{s\text{-}o}^{k}$, Φ_{h}^{io}, and $\Phi_{m,1}^{k}$ phases observed in the dendronized PBI with n = 9. The experimental density (Table 2) in combination with the lattice parameters demonstrated that the unit cell of the $\Phi_{m,1}^{k}$ phase contains four columns with an estimated diameter of ~38 Å. This value is close to the diameter of 38.9 and 37.5 Å of the supramolecular columns forming the $\Phi_{s\text{-}o}^{k}$ and Φ_{h}^{io} phases (Figure 11). This analysis shows that the column stratum with a thickness of 3.5 Å is generated by two side by side dendronized

PBIs. Although the assessment of the space group of the $\Phi_{m,1}^{k}$ phase is not yet definitive, one possible mechanism to generate this unusual four column unit cell is illustrated in Figure 11. Inspired by the observation that the packing of the low temperature $\Phi_{s\text{-}o}^{k}$ phases consists of adjacent rows of columns with a relative registry shift (Figure 11b), most probable is that a similar registry shift can induce a doubling of the unit cell and generate the four columns repeat unit illustrated in Figure 11c. Interestingly, the scattering intensity of the fourth line is significantly larger than the intensity of the eighth line, as indicated in the WAXS fiber pattern presented in Figure 7. This suggests that the packing of dendronized perylenes into supramolecular tetramers established for the $\Phi_{s\text{-}o}^{k}$ and Φ_{h}^{io} phases is most probably preserved upon the slow transition from Φ_{h}^{io} to $\Phi_{m,1}^{k}$ phase. Considering that these equatorial diffractions can be generated by intra- and intercolumnar correlations, it is difficult to separate their individual contributions. Therefore, the proposed preservation of the tetramer packing is just one possible solution.

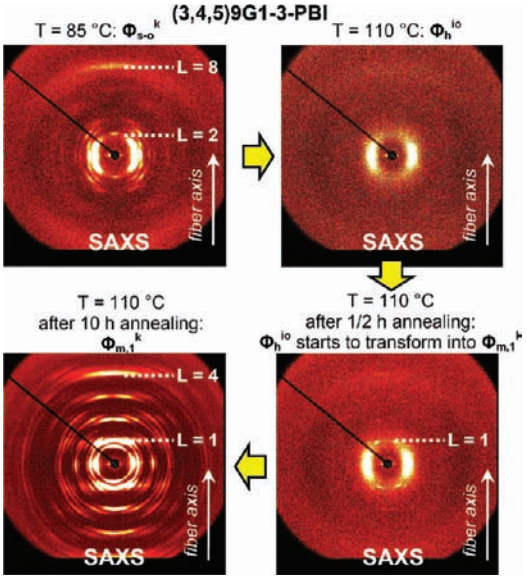

Figure 9. The small-angle XRD fiber patterns collected in the second heating scans of (3,4,5)9G1-3-PBI following the indicated thermal cycle illustrating the transformation of the Φ_{h}^{io} into $\Phi_{m,1}^{k}$ upon annealing.

Scheme 3a details the change of the supramolecular arrangement within the complex helical columns generated by dimers of (3,4,5)12G1-1-PBI via the Φ_{h}^{io} to $\Phi_{m,1}^{k}$ transition. This transition is accompanied by the formation of long-range intercolumnar order via coupling of the supramolecular columns. During this transition, the intra- and interdimer 3.5 Å $\pi-\pi$ stacking distance is preserved (Scheme 3a). Consequently, although the dendritic periphery of the supramolecular helical column undergoes significant packing changes to accommodate strong 3D coupling between the columns via the change from alternating up−down arrangement of dendronized PBIs in Φ_{h}^{io} phase to all up or all down in the $\Phi_{m,1}^{k}$ phase, their PBI fragments undergo rotational changes but no translational changes. At the same time, the helical columns assembled from tetramers of n = 8, 9, m = 3, and the PBI cores undergo both rotational and translational changes at the transition from Φ_{h}^{io} to $\Phi_{m,1}^{k}$ (Scheme 3b). Most probably, the self-repairing process form alternating $\pi-\pi$ stacking of 3.5 and 4.1 Å in the Φ_{h}^{io} phase to 3.5 Å $\pi-\pi$ stacking in the $\Phi_{m,1}^{k}$ phase of n = 8, 9, m = 3 was facilitated by the strong 3D coupling of the helical columns (Scheme 3b). A close-packed 3.5 Å $\pi-\pi$ stacking of the PBIs and stronger 3D coupling of the supramolecular columns in the

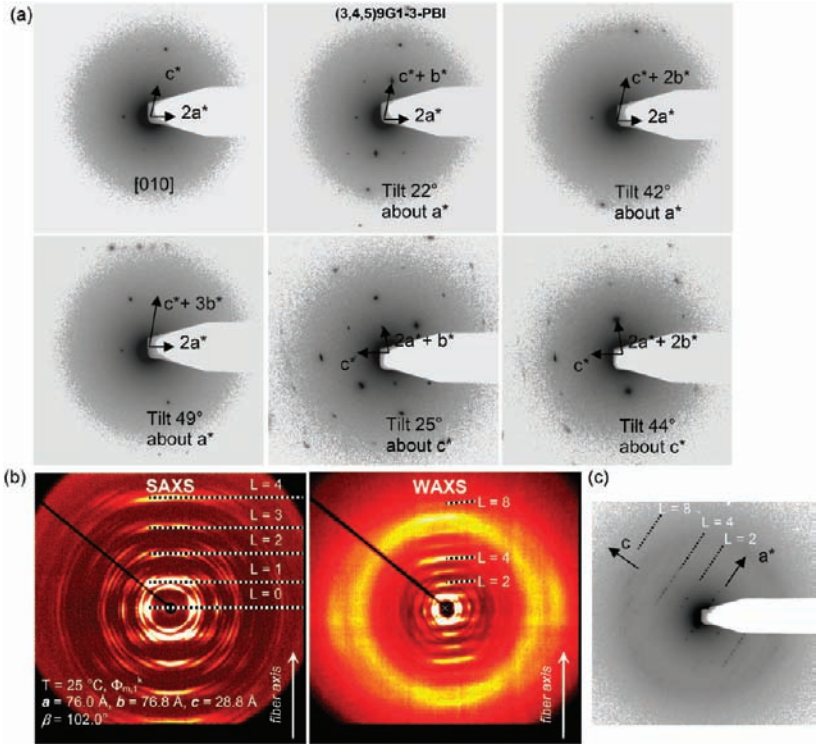

Figure 10. Electron diffraction (a,c) and XRD patterns (b) collected in the $\Phi_{m,1}^{k}$ self-organized from (3,4,5)9G1-3-PBI.

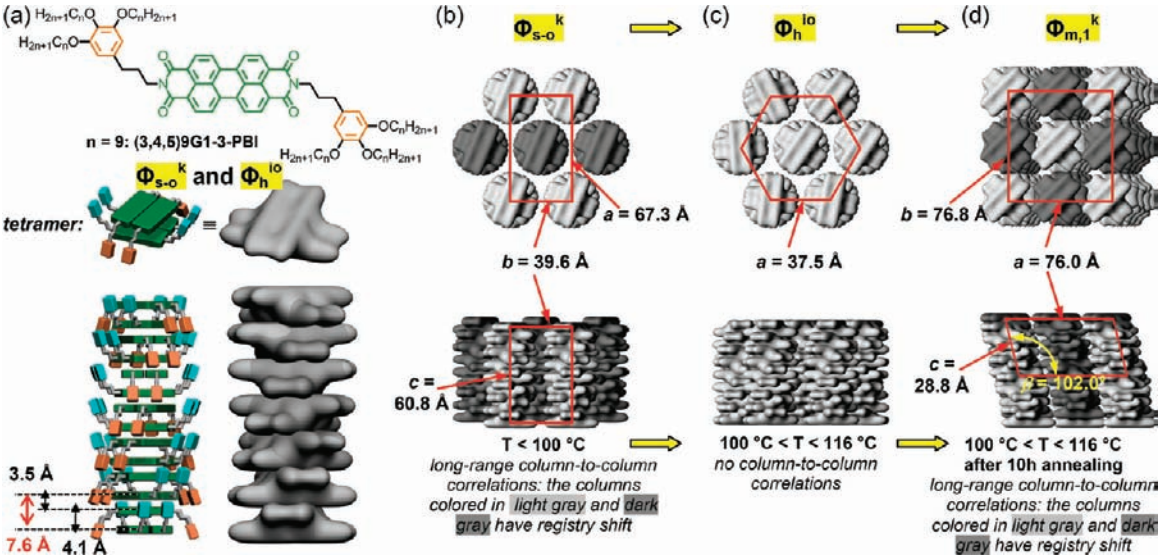

Figure 11. Assembly of the helical complex columns from tetramers of (3,4,5)9G1-3-PBI, forming the $\Phi_{s\text{-}o}{}^{k}$ and $\Phi_{h}{}^{io}$ phases (a), and details of the $\Phi_{s\text{-}o}{}^{k}$ (b), $\Phi_{h}{}^{io}$ (c), and $\Phi_{m,1}{}^{k}$ (d) lattices. The possible registry shift of the supramolecular columns that can explain the unusual four column unit cell of the $\Phi_{m,1}{}^{k}$ phase is shown in (d).

Scheme 3. Self-Repairing Complex Helical Columns Generated from Dimers (a) and Tetramers (b) of Dendronized PBIs

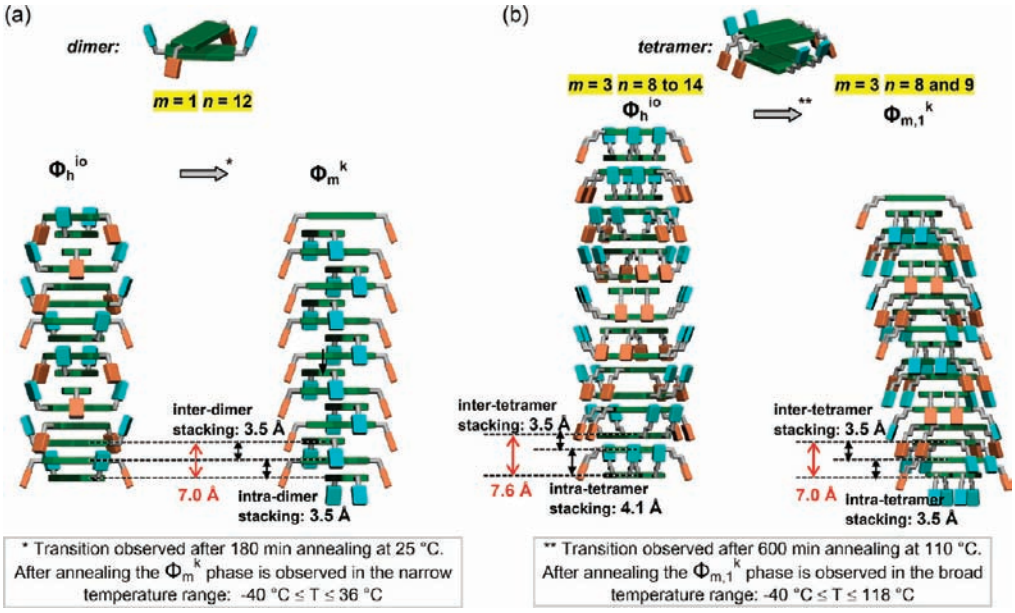

$\Phi_{m,1}{}^{k}$ phase at the transition from the $\Phi_{s\text{-}o}{}^{k}$ phase is also demonstrated by the significant increase of the enthalpy change associated with the transition from the $\Phi_{m,1}{}^{k}$ phase to the isotropic phase (Figure 3b,c). The ΔH = 2.73 kcal/mol associated with the $\Phi_{m,1}{}^{k}$—i transition is 87% larger than the ΔH = 1.1 + 0.36 = 1.46 kcal/mol associated with the combined $\Phi_{s\text{-}o}{}^{k}$ to $\Phi_{h}{}^{io}$ to i transitions (Figure 3b).

The self-repairing process of the helical columns generated from dimers and from tetramers of dendronized PBIs takes place only upon annealing in their 2D $\Phi_{h}{}^{io}$ liquid crystalline phase. Variable-temperature solid-state ^{1}H NMR technique provided additional insight into this self-repairing process, as detailed in the next subsection.

Analysis of the $\Phi_{h}{}^{io}$ to $\Phi_{m,1}{}^{k}$ Slow Phase Transition and the Self-Repairing Process of (3,4,5)9G1-3-PBI by Variable-Temperature Solid-State ^{1}H NMR. Variable-temperature ^{1}H NMR analysis[15] carried out on oriented samples of (3,4,5)9G1-3-PBI is shown in Figure 12. In the first heating of the fiber extruded in the $\Phi_{s\text{-}o}{}^{k}$ phase, the ^{1}H NMR exhibits broad spectra in the aromatic region, identical to those of the (3,4,5)12G1-3-PBI reported previously.[10] In the temperature range from 50 to 100 °C, the ^{1}H NMR spectra in the aromatic region exhibit a low but detectable mobility. After heating above 100 °C, into the $\Phi_{h}{}^{io}$ phase, the ^{1}H NMR spectra exhibit the same line narrowing observed previously in the n = 12, m = 3,[10] which was explained with the help of computer simulation[15] via a mechanism where

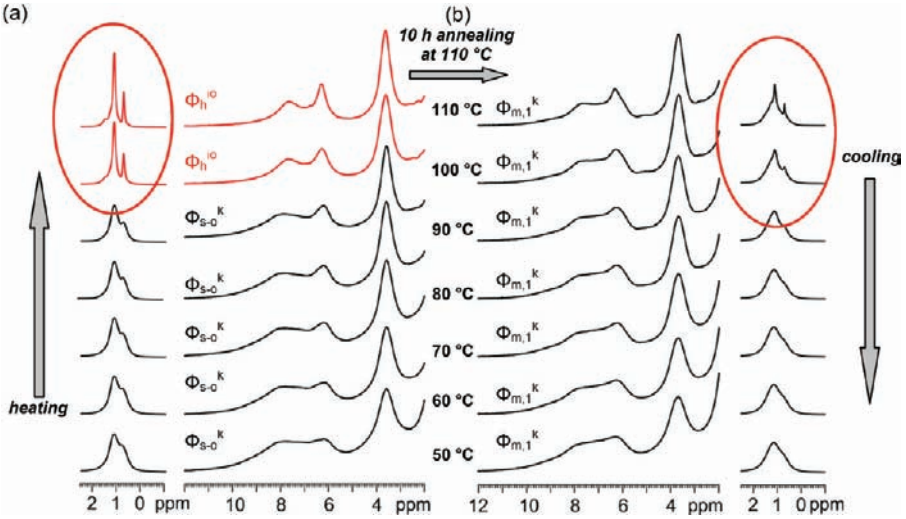

Figure 12. Variable-temperature ^{1}H MAS spectra of (3,4,5)9G1-3-PBI recorded at 25 kHz MAS and 700 MHz ^{1}H Larmor frequency in the heating (a) and cooling (b) experiments performed with a rate of 1 °C/min. The data from (b) were collected after 10 h of annealing at 110 °C in the Φ_h^{io} phase. The aliphatic signals of the two phases are reduced by a factor 1/25 in intensity for better comparison.

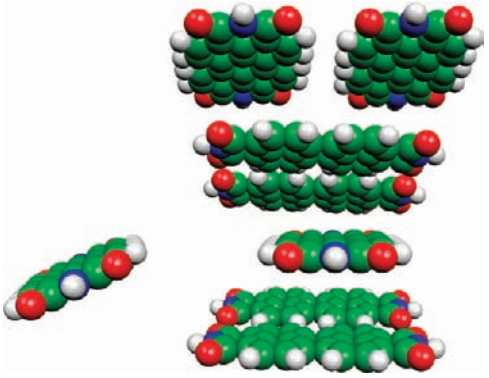

Figure 13. Schematic of the mechanism[10] that mediates the slow $\Phi_h^{io}-\Phi_{m,1}^{k}$ transition and the self-repairing process established for (3,4,5)9G1-3-PBI.

the molecules leave the supramolecular column, flip over, and re-enter a column at a later time (Figure 13). The line narrowing of the core proton around 7−8 ppm is particularly clear in the Φ_h^{io} phase (Figure 12a). Therefore, the increased mobility, demonstrated by the line narrowing of the ^{1}H NMR spectra at the $\Phi_{s\text{-}o}^{k}$ to Φ_h^{io} transition (Figure 12a), is characteristic both for the PBI core and for the side groups.

After annealing the oriented sample of (3,4,5)9G1-3-PBI for 10 h at 110 °C in the Φ_h^{io} phase, the ^{1}H NMR spectra collected upon cooling in the $\Phi_{m,1}^{k}$ phase (Figure 12b) do not exhibit the temperature-dependent line narrowing observed in the first heating (Figure 12a). In addition, the signals of the core protons are shifted slightly toward low ppm values by ∼0.2−0.3 ppm. This result indicate a better $\pi-\pi$ stacking in the $\Phi_{m,1}^{k}$ phase, in excellent agreement with the changes of the stacking distances of the dendronized PBIs established by XRD from alternating 3.5 and 4.1 Å distances in the $\Phi_{s\text{-}o}^{k}$ and Φ_h^{io} phases to only a single 3.5 Å distance in the 3D $\Phi_{m,1}^{k}$ phase (Scheme 3b). The very narrow signals observed around 1 ppm in the ^{1}H NMR spectra collected in the Φ_h^{io} phase (marked by the red circle in Figure 12a) were also observed after annealing on top of the broad signals of the $\Phi_{m,1}^{k}$ phase (Figure 12b). This result can be explained by a slight temperature gradient throughout the sample, which can transform parts of the sample into an isotropic melt. Note that in another variable-temperature experiment (data not shown) the overall ^{1}H NMR spectra were similar to the data reported in Figure 12, but the very narrow signal indicated by the red circle in Figure 12b was not observed. Therefore, the variable-temperature solid-state ^{1}H NMR data demonstrate that the formation of the highly ordered $\Phi_{m,1}^{k}$ phase after annealing into the Φ_h^{io} phase is accompanied by a reduction of the molecular dynamics of the outer alkyl chains and better $\pi-\pi$ stacking. This complex dynamics, in which dendronized PBI can leave the column, rotate, and enter the same or another column,[10] provides a route to the $\Phi_h^{io}-\Phi_{m,1}^{k}$ slow transition and for the self-repairing process.

CONCLUSIONS

A previous publication from our laboratory[10] reported the discovery of a dendronized PBI (3,4,5)12G1-3-PBI that self-assembles into a complex helical column generated from tetramers containing a pair of two molecules arranged side-by-side and another pair in the next stratum of the column, turned upside-down, and rotated around the column axis at an intratetramer angle that is different from that of the intertetramer angle. In addition, the intratetramer stacking distance in this column is 4.1 Å, while the intertetramer distance is 3.5 Å. At high temperature, this helical column self-organizes in a 2D Φ_h^{io} phase that represents the thermodynamic product, which is assembled by a thermodynamically controlled process. At low temperature, the same column self-organizes in a 3D $\Phi_{s\text{-}o}^{k}$ phase via a kinetically controlled process, although this phase represents the thermodynamic product. The architecture of this complex helical column, the structure of its 3D periodic array, and its kinetically controlled self-organization are not ideal for the design of supramolecular structures with high charge carrier mobility, and, as expected, the mobility of electrons in this sample is moderate.[9g] Therefore, a library of 11 (3,4,5)*n*G1-3PBIs with n = 14−4 was synthesized and the supramolecular assemblies

generated were analyzed in an attempt to discover the n value that will transform the kinetically controlled self-assembly of the $\Phi_{s\text{-}o}{}^{k}$ phase into a thermodynamically controlled process. These experiments demonstrated that for n = 11, 10, 9, and 8, indeed the assembly of the 3D $\Phi_{s\text{-}o}{}^{k}$ phase starts to become thermodynamically controlled, while for n = 12−14 the 3D phases from low temperature remain kinetically controlled. However, the most important discovery is that for n = 9 and 8, the assembly of the 3D $\Phi_{s\text{-}o}{}^{k}$ phase first transforms from a kinetically controlled (for n = 12−14) into a thermodynamically controlled. Subsequently, the $\Phi_{s\text{-}o}{}^{k}$ structure becomes the kinetic product because the new 3D higher-order $\Phi_{m,1}{}^{k}$ phase is the new thermodynamic product that is assembled via a kinetically controlled complex process. This process was elucidated by a combination of solid-state NMR and XRD experiments. Even more important and unexpected, in this new $\Phi_{m,1}{}^{k}$ phase the helical columns are self-repaired and exhibit an intratetramer stacking distance equal to that of the intertetramer distance of 3.5 Å. Therefore, this self-repairing process transforms the two different intra- and intertetramer stacking distances into a single one that is suitable for the generation of high charge carrier mobility. This self-repairing process takes place only by annealing in the 2D $\Phi_{h}{}^{io}$ phase and resembles related self-repairing processes reported previously.[13f] The new $\Phi_{m,1}{}^{k}$ thermodynamic product, its self-assembly via a kinetically controlled process, together with the self-repairing process of the complex helical columns reported here are important both for the understanding of the mechanisms of self-assembly and for the molecular design of high charge carrier mobility in supramolecular electronic materials. The physical properties of the racemic and enantiomerically pure helical columns are of significant interest[16] and are under investigation. The dendronized PBIs with n = 4−7 self-organize via a kinetically controlled process in another 3D $\Phi_{m,2}{}^{k}$ thermodynamic product generated from helical columns that are not yet elucidated. These experiments and the research strategy involved demonstrate the power of the library approach[12,13] to discovery. It remains to be seen if the prediction[12m−o] of the 3D architectures required for special electronic applications will be possible.

■ ASSOCIATED CONTENT

Supporting Information. Experimental procedures with complete spectral and structural analysis, and complete refs 10 and 12l. This material is available free of charge via the Internet at http://pubs.acs.org.

■ AUTHOR INFORMATION

Corresponding Author
percec@sas.upenn.edu

■ ACKNOWLEDGMENT

Financial support by the National Science Foundation (DMR-0548559, DMR-0520020, DMR-1066116, and DMS-0935165), the Humboldt Foundation, and the P. Roy Vagelos Chair at Penn is gratefully acknowledged. This work was also financially supported by the German Research Foundation (DFG) through grant SFB 625, by the European FP7 Project NANOGOLD (grant 228455), and by the WCU Program funded by the Ministry of Education, Science, and Technology of Korea (R31-10013).

■ REFERENCES

(1) (a) Würthner, F.; Stolte, M. *Chem. Commun.* **2011**, *47*, 5109–5115. (b) Würthner, F.; Kaiser, T. E.; Saha-Möller, C. R. *Angew. Chem., Int. Ed.* **2011**, *50*, 3376–3410. (c) Huang, C.; Barlow, S.; Marder, S. R. *J. Org. Chem.* **2011**, *76*, 2386–2407. (d) Usta, H.; Facchetti, A.; Marks, T. J. *Acc. Chem. Res.* **2011**, *44*, 501–510. (e) Chen, Z. J.; Lohr, A.; Saha-Möller, C. R.; Würthner, F. *Chem. Soc. Rev.* **2009**, *38*, 564–584. (f) Würthner, F. *Chem. Commun.* **2004**, 1564–1579. (g) Langhals, H. *Heterocycles* **1995**, *40*, 477–500.

(2) (a) Zhan, X. W.; Facchetti, A.; Barlow, S.; Marks, T. J.; Ratner, M. A.; Wasielewski, M. R.; Marder, S. R. *Adv. Mater.* **2011**, *23*, 268–284. (b) Carsten, B.; He, F.; Son, H. J.; Xu, T.; Yu, L. *Chem. Rev.* **2011**, *111*, 1493–1528. (c) Weissman, H.; Ustinov, A.; Shimoni, E.; Cohen, S. R.; Rybtchinski, B. *Polym. Adv. Technol.* **2011**, *22*, 133–138. (d) Anthony, J. E.; Facchetti, A.; Heeney, M.; Marder, S. R.; Zhan, X. *Adv. Mater.* **2010**, *22*, 3876–3892. (e) Zhan, X.; Tan, Z. A.; Zhou, E. J.; Li, Y. F.; Misra, R.; Grant, A.; Domercq, B.; Zhang, X. H.; An, Z. S.; Zhang, X.; Barlow, S.; Kippelen, B.; Marder, S. R. *J. Mater. Chem.* **2009**, *19*, 5794–5803. (f) Zhan, X.; Tan, Z.; Domercq, B.; An, Z.; Zhang, X.; Barlow, S.; Li, Y.; Zhu, D.; Kippelen, B.; Marder, S. R. *J. Am. Chem. Soc.* **2007**, *129*, 7246–7247. (g) Blanco, R.; Gomez, R.; Seoane, C.; Segura, J. L.; Mena-Osteritz, E.; Bauerle, P. *Org. Lett.* **2007**, *9*, 2171–2174. (h) Facchetti, A. *Chem. Mater.* **2011**, *23*, 733–758.

(3) (a) Wasielewski, M. R. *Acc. Chem. Res.* **2009**, *42*, 1910–1921. (b) Sinks, L. E.; Rybtchinski, B.; Iimura, M.; Jones, B. A.; Goshe, A. J.; Zuo, X. B.; Tiede, D. M.; Li, X. Y.; Wasielewski, M. R. *Chem. Mater.* **2005**, *17*, 6295–6303. (c) Fuller, M. J.; Sinks, L. E.; Rybtchinski, B.; Giaimo, J. M.; Li, X. Y.; Wasielewski, M. R. *J. Phys. Chem. A* **2005**, *109*, 970–975. (d) Rosen, B. M.; Wilson, C. J.; Wilson, D. A.; Peterca, M.; Imam, M. R.; Percec, V. *Chem. Rev.* **2009**, *109*, 6275–6540. (e) Percec, V.; Aqad, E.; Peterca, M.; Imam, M. R.; Glodde, M.; Bera, T. K.; Miura, Y.; Balagurusamy, V. S. K.; Ewbank, P. C.; Würthner, F.; Heiney, P. A. *Chem.-Eur. J.* **2007**, *13*, 3330–3345.

(4) (a) *Supramolecular Dye Chemistry*; Würthner, F., Ed.; Topics in Current Chemistry 258; Springer-Verlag: Berlin, 2005. (b) Zollinger, H. *Color Chemistry*, 3rd ed.; Wiley-VCH: Weinheim, 2003. (c) Herbst, W.; Hunger, K. *Industrial Organic Pigments: Production, Properties, Applications*, 3rd ed.; Wiley-VCH: Weinheim, 2004. (d) Klebe, G.; Graser, F.; Hädicke, E.; Berndt, J. *Acta Crystallogr., Sect. B* **1989**, *45*, 69–77. (e) Graser, F.; Hädicke, E. *Liebigs Ann. Chem.* **1980**, 1994–2011. (f) Graser, F.; Hädicke, E. *Liebigs Ann. Chem.* **1984**, 483–494.

(5) Law, K. Y. *Chem. Rev.* **1993**, *93*, 449–486.

(6) (a) Zang, L.; Liu, R. C.; Holman, M. W.; Nguyen, K. T.; Adams, D. M. *J. Am. Chem. Soc.* **2002**, *124*, 10640–10641. (b) Baumstark, D.; Wagenknecht, H.-A. *Angew. Chem., Int. Ed.* **2008**, *47*, 2612–2614. (c) Zhang, X.; Chen, Z. J.; Würthner, F. *J. Am. Chem. Soc.* **2007**, *129*, 4886–4887. (d) Zhang, X.; Rehm, S.; Safont-Sempere, M. M.; Würthner, F. *Nat. Chem.* **2009**, *1*, 623–629.

(7) (a) Qu, J. Q.; Pschirer, N. G.; Liu, D. J.; Stefan, A.; De Schryver, F. C.; Mullen, K. *Chem.-Eur. J.* **2004**, *10*, 528–537. (b) Cotlet, M.; Masuo, S.; Lor, M.; Fron, E.; Van der Auweraer, M.; Mullen, K.; Hofkens, J.; De Schryver, F. *Angew. Chem., Int. Ed.* **2004**, *43*, 6116–6120. (c) Kaiser, T. E.; Wang, H.; Stepanenko, V.; Würthner, F. *Angew. Chem., Int. Ed.* **2007**, *46*, 5541–5544. (d) Kaiser, T. E.; Stepanenko, V.; Würthner, F. *J. Am. Chem. Soc.* **2009**, *131*, 6719–6732.

(8) (a) Fischer, M. K. R.; Kaiser, T. E.; Würthner, F.; Bauerle, P. *J. Mater. Chem.* **2009**, *19*, 1129–1141. (b) Backes, C.; Schmidt, C. D.; Hauke, F.; Bottcher, C.; Hirsch, A. *J. Am. Chem. Soc.* **2009**, *131*, 2172–2184. (c) Heek, T.; Fasting, C.; Rest, C.; Zhang, X.; Würthner, F.; Haag, R. *Chem. Commun.* **2010**, *46*, 1884–1886. (d) Schmidt, C. D.; Bottcher, C.; Hirsch, A. *Eur. J. Org. Chem.* **2009**, 5337–5349. (e) Backes, C.; Schmidt, C. D.; Rosenlehner, K.; Hauke, F.; Coleman, J. N.; Hirsch, A. *Adv. Mater.* **2010**, *22*, 788–802. (f) Würthner, F.; Thalacker, C.; Diele, S.; Tschierske, C. *Chem.-Eur. J.* **2001**, *7*, 2245–2253. (g) van Herrikhuyzen, J.; Syamakumari, A.; Schenning, A.; Meijer, E. W. *J. Am. Chem. Soc.* **2004**, *126*, 10021–10027. (h) Würthner, F.; Chen, Z. J.; Hoeben, F. J. M.; Osswald, P.; You, C. C.; Jonkheijm, P.; von Herrikhuyzen, J.; Schenning, A.; van der Schoot, P.; Meijer, E. W.; Beckers, E. H. A.; Meskers, S. C. J.; Janssen, R. A. J. *J. Am. Chem. Soc.* **2004**, *126*,

10611–10618. (i) Chen, Z.; Baumeister, U.; Tschierske, C.; Würthner, F. *Chem.-Eur. J.* **2007**, *13*, 450–465. (j) Würthner, F.; Chen, Z. J.; Dehm, V.; Stepanenko, V. *Chem. Commun.* **2006**, 1188–1190. (k) Chen, Z. J.; Stepanenko, V.; Dehm, V.; Prins, P.; Siebbeles, L. D. A.; Seibt, J.; Marquetand, P.; Engel, V.; Würthner, F. *Chem.-Eur. J.* **2007**, *13*, 436–449. (l) Debije, M. G.; Chen, Z. J.; Piris, J.; Neder, R. B.; Watson, M. M.; Mullen, K.; Würthner, F. *J. Mater. Chem.* **2005**, *15*, 1270–1276. (m) Li, X.-Q.; Stepanenko, V.; Chen, Z. J.; Prins, P.; Siebbeles, L. D. A.; Würthner, F. *Chem. Commun.* **2006**, 3871–3873. (n) Li, X.-Q.; Zhang, X.; Ghosh, S.; Würthner, F. *Chem.-Eur. J.* **2008**, *14*, 8074–8078.

(9) (a) Cormier, R. A.; Gregg, B. A. *J. Phys. Chem. B* **1997**, *101*, 11004–11006. (b) Cormier, R. A.; Gregg, B. A. *Chem. Mater.* **1998**, *10*, 1309–1319. (c) An, Z. S.; Yu, J. S.; Jones, S. C.; Barlow, S.; Yoo, S.; Domercq, B.; Prins, P.; Siebbeles, L. D. A.; Kippelen, B.; Marder, S. R. *Adv. Mater.* **2005**, *17*, 2580–2583. (d) Shoaee, S.; An, Z. S.; Zhang, X.; Barlow, S.; Marder, S. R.; Duffy, W.; Heeney, M.; McCulloch, I.; Durrant, J. R. *Chem. Commun.* **2009**, 5445–5447. (e) An, Z. Z.; Yu, J. S.; Domercq, B.; Jones, S. C.; Barlow, S.; Kippelen, B.; Marder, S. R. *J. Mater. Chem.* **2009**, *19*, 6688–6698. (f) Dehm, V.; Chen, Z. J.; Baumeister, U.; Prins, P.; Siebbeles, L. D. A.; Würthner, F. *Org. Lett.* **2007**, *9*, 1085–1088. (g) Duzhko, V.; Aqad, E.; Imam, M. R.; Peterca, M.; Percec, V.; Singer, K. D. *Appl. Phys. Lett.* **2008**, *92*, 113312.

(10) Percec, V.; et al. *J. Am. Chem. Soc.* **2011**, *133*, 12197–12219.

(11) (a) Hasenknopf, B.; Lehn, J. M.; Boumediene, N.; Leize, E.; Van Dorsselaer, A. *Angew. Chem., Int. Ed.* **1998**, *37*, 3265–3268. (b) Philp, D.; Stoddart, J. F. *Angew. Chem., Int. Ed. Engl.* **1996**, *35*, 1155–1196. (c) Kidd, T. J.; Leigh, D. A.; Wilson, A. J. *J. Am. Chem. Soc.* **1999**, *121*, 1599–1600. (d) Ashton, P. R.; Glink, P. T.; Martinez Diaz, M. V.; Stoddart, J. F.; White, A. J. P.; Williams, D. J. *Angew. Chem., Int. Ed. Engl.* **1996**, *35*, 1930–1933. (e) Lubrich, D.; Green, S. J.; Turberfield, A. J. *J. Am. Chem. Soc.* **2009**, *131*, 2422–2423. (f) Northrop, B. H.; Khan, S. J.; Stoddart, J. F. *Org. Lett.* **2006**, *8*, 2159–2162. (g) Nguyen, H. D.; Reddy, V. S.; Brooks, C. L. *Nano Lett.* **2007**, *7*, 338–344. (h) Cui, H.; Chen, Z.; Zhong, S.; Wooley, K. L.; Pochan, D. J. *Science* **2007**, *317*, 647–650.

(12) (a) Percec, V.; Cho, W. D.; Ungar, G.; Yeardley, D. J. P. *J. Am. Chem. Soc.* **2001**, *123*, 1302–1315. (b) Percec, V.; Mitchell, C. M.; Cho, W. D.; Uchida, S.; Glodde, M.; Ungar, G.; Zeng, X. B.; Liu, Y. S.; Balagurusamy, V. S. K.; Heiney, P. A. *J. Am. Chem. Soc.* **2004**, *126*, 6078–6094. (c) Percec, V.; Peterca, M.; Sienkowska, M. J.; Ilies, M. A.; Aqad, E.; Smidrkal, J.; Heiney, P. A. *J. Am. Chem. Soc.* **2006**, *128*, 3324–3334. (d) Percec, V.; Holerca, M. N.; Nummelin, S.; Morrison, J. L.; Glodde, M.; Smidrkal, J.; Peterca, M.; Rosen, B. M.; Uchida, S.; Balagurusamy, V. S. K.; Sienkowska, M. L.; Heiney, P. A. *Chem.-Eur. J.* **2006**, *12*, 6216–6241. (e) Percec, V.; Won, B. C.; Peterca, M.; Heiney, P. A. *J. Am. Chem. Soc.* **2007**, *129*, 11265–11278. (f) Percec, V.; Peterca, M.; Dulcey, A. E.; Imam, M. R.; Hudson, S. D.; Nummelin, S.; Adelman, P.; Heiney, P. A. *J. Am. Chem. Soc.* **2008**, *130*, 13079–13094. (g) Percec, V.; Imam, M. R.; Peterca, M.; Wilson, D. A.; Heiney, P. A. *J. Am. Chem. Soc.* **2009**, *131*, 1294–1304. (h) Percec, V.; Imam, M. R.; Peterca, M.; Wilson, D. A.; Graf, R.; Spiess, H. W.; Balagurusamy, V. S. K.; Heiney, P. A. *J. Am. Chem. Soc.* **2009**, *131*, 7662–7677. (i) Percec, V.; Imam, M. R.; Peterca, M.; Cho, W.-D.; Heiney, P. A. *Isr. J. Chem.* **2009**, *49*, 55–70. (j) Peterca, M.; Imam, M. R.; Leowanawat, P.; Rosen, B. M.; Wilson, D. A.; Wilson, C. J.; Zeng, X.; Ungar, G.; Heiney, P. A.; Percec, V. *J. Am. Chem. Soc.* **2010**, *132*, 11288–11305. (k) Rosen, B. M.; Peterca, M.; Huang, C.; Zeng, X.; Ungar, G.; Percec, V. *Angew. Chem., Int. Ed.* **2010**, *49*, 7002–7005. (l) Percec, V.; et al. *Science* **2010**, *328*, 1009–1014. (m) Rosen, B. M.; Wilson, D. A.; Wilson, C. J.; Peterca, M.; Won, B. C.; Huang, C.; Lipski, L. R.; Zeng, X.; Ungar, G.; Heiney, P. A.; Percec, V. *J. Am. Chem. Soc.* **2009**, *131*, 17500–17521. (n) Tomalia, D. A. *J. Nanopart. Res.* **2009**, *11*, 1251–1310. (o) Tomalia, D. A. *Soft Matter* **2010**, *6*, 456–474.

(13) (a) Balagurusamy, V. S. K.; Ungar, G.; Percec, V.; Johansson, G. *J. Am. Chem. Soc.* **1997**, *119*, 1539–1555. (b) Hudson, S. D.; Jung, H.-T.; Percec, V.; Cho, W.-D.; Johansson, G.; Ungar, G.; Balagurusamy, V. S. K. *Science* **1997**, *278*, 449–452. (c) Percec, V.; Ahn, C. H.; Ungar, G.; Yeardley, D. J. P.; Möller, M.; Sheiko, S. S. *Nature* **1998**, *391*, 161–164. (d) Percec, V.; Cho, W.-D.; Möller, M.; Prokhorova, S. A.; Ungar, G.; Yeardley, D. J. P. *J. Am. Chem. Soc.* **2000**, *122*, 4249–4250. (e) Yeardley, D. J. P.; Ungar, G.; Percec, V.; Holerca, M. N.; Johansson, G. *J. Am. Chem. Soc.* **2000**, *122*, 1684–1689. (f) Percec, V.; Glodde, M.; Bera, T. K.; Miura, Y.; Shiyanovskaya, I.; Singer, K. D.; Balagurusamy, V. S. K.; Heiney, P. A.; Schnell, I.; Rapp, A.; Spiess, H. W.; Hudson, S. D.; Duan, H. *Nature* **2002**, *419*, 384–387. (g) Ungar, G.; Liu, Y.; Zeng, X.; Percec, V.; Cho, W. D. *Science* **2003**, *299*, 1208–1211. (h) Percec, V.; Dulcey, A. E.; Balagurusamy, V. S. K.; Miura, Y.; Smidrkal, J.; Peterca, M.; Nummelin, S.; Edlund, U.; Hudson, S. D.; Heiney, P. A.; Hu, D. A.; Magonov, S. N.; Vinogradov, S. A. *Nature* **2004**, *430*, 764–768. (i) Zeng, X.; Ungar, G.; Liu, Y.; Percec, V.; Dulcey, S. E.; Hobbs, J. K. *Nature* **2004**, *428*, 157–160.

(14) (a) Ungar, G.; Abramic, D.; Percec, V.; Heck, J. A. *Liq. Cryst.* **1996**, *21*, 73–86. (b) Percec, V.; Ahn, C. H.; Bera, T. K.; Ungar, G.; Yeardley, D. J. P. *Chem.-Eur. J.* **1999**, *5*, 1070–1083. (c) Percec, V.; Bera, T. K.; Glodde, M.; Fu, Q. Y.; Balagurusamy, V. S. K.; Heiney, P. A. *Chem.-Eur. J.* **2003**, *9*, 921–935. (d) Percec, V.; Peterca, M.; Yurchenko, M. E.; Rudick, J. G.; Heiney, P. A. *Chem.-Eur. J.* **2008**, *14*, 909–918. (e) Percec, V.; Rudick, J. G.; Peterca, M.; Yurchenko, M. E.; Smidrkal, J.; Heiney, P. A. *Chem.-Eur. J.* **2008**, *14*, 3355–3362.

(15) (a) Brown, S. P.; Spiess, H. W. *Chem. Rev.* **2001**, *101*, 4125–4155. (b) Schmidt, J.; Hoffmann, A.; Spiess, H. W.; Sebastiani, D. *J. Phys. Chem. B* **2006**, *110*, 23204–23210. (c) Ochsenfeld, C.; Brown, S. P.; Schnell, I.; Gauss, J.; Spiess, H. W. *J. Am. Chem. Soc.* **2001**, *123*, 2597–2606. (d) Hansen, M. R.; Graf, R.; Sekharan, S.; Sebastiani, D. *J. Am. Chem. Soc.* **2009**, *131*, 5251–5256. (e) Fritzsche, M.; Bohle, A.; Dudenko, D.; Baumeister, U.; Sebastiani, D.; Richardt, G.; Spiess, H. W.; Hansen, M. R.; Hoeger, S. *Angew. Chem., Int. Ed.* **2011**, *50*, 3030–3033.

(16) (a) Safont-Sempere, M. M.; Osswald, P.; Radacki, K.; Würthner, F. *Chem.-Eur. J.* **2010**, *16*, 7380–7384. (b) Rosen, B. M.; Peterca, M.; Morimitsu, K.; Dulcey, A. E.; Leowanawat, P.; Resmerita, A.-M.; Imam, M. R.; Percec, V. *J. Am. Chem. Soc.* **2011**, *133*, 5135–5151. (c) Safont-Sempere, M. M.; Stepanenko, V.; Lehmann, M.; Würthner, F. *J. Mater. Chem.* **2011**, *21*, 7201–7209.